








General trends of superconducting pairing and magnetic correlations in the Ruddlesden-Popper nickelate m -layered superconductors $\text{La}_{m+1}\text{Ni}_m\text{O}_{3m+1}$

Yang Zhang ¹, Ling-Fang Lin ^{1,*}, Adriana Moreo ^{1,2}, Satoshi Okamoto ², Thomas A. Maier ^{3,†} and Elbio Dagotto ^{1,2,‡}

¹*Department of Physics and Astronomy, University of Tennessee, Knoxville, Tennessee 37996, USA*

²*Materials Science and Technology Division, Oak Ridge National Laboratory, Oak Ridge, Tennessee 37831, USA*

³*Computational Sciences and Engineering Division, Oak Ridge National Laboratory, Oak Ridge, Tennessee 37831, USA*

 (Received 18 April 2025; revised 27 July 2025; accepted 2 September 2025; published 23 September 2025)

We report a comprehensive theoretical analysis of the Ruddlesden-Popper layered nickelates $\text{La}_{m+1}\text{Ni}_m\text{O}_{3m+1}$ ($m = 1$ to 6) under pressure. These materials have recently received significant attention due to the discovery of superconductivity in some nickelates under pressure. Our results suggest that, while these Ruddlesden-Popper layered nickelates display many similarities, they also show noticeable differences. One of the common features of $\text{La}_{m+1}\text{Ni}_m\text{O}_{3m+1}$ is that the electronic states near the Fermi level are mainly contributed by Ni $3d$ orbitals, slightly hybridized with O $2p$ orbitals. The Ni $d_{3z^2-r^2}$ orbitals display bonding-antibonding, or bonding-antibonding-nonbonding, characteristic splittings, depending on the even or odd number of stacking layers m . In addition, the ratio of the in-plane interorbital hopping between $d_{3z^2-r^2}$ and $d_{x^2-y^2}$ orbitals and in-plane intraorbital hopping between $d_{x^2-y^2}$ orbitals was found to be large in $\text{La}_{m+1}\text{Ni}_m\text{O}_{3m+1}$ ($m = 1$ to 6), and this ratio increases from $m = 1$ to $m = 6$, suggesting that the in-plane hybridization will increase as the layer number m increases. In contrast to the dominant s^\pm -wave state driven by spin fluctuations in the bilayer $\text{La}_3\text{Ni}_2\text{O}_7$ and trilayer $\text{La}_4\text{Ni}_3\text{O}_{10}$, two nearly degenerate $d_{x^2-y^2}$ -wave and s^\pm -wave leading states were obtained in the four-layer stacking $\text{La}_5\text{Ni}_4\text{O}_{13}$ and five-layer stacking $\text{La}_6\text{Ni}_5\text{O}_{16}$. The leading s^\pm -wave state was recovered in the six-layer material $\text{La}_7\text{Ni}_6\text{O}_{19}$ with slightly higher calculated pairing strength λ than that of the $d_{x^2-y^2}$ -wave state. All this evidence suggests that both s^\pm -wave and $d_{x^2-y^2}$ -wave channels are strongly competing in the high-order nickelates based on our random-phase approximation calculations. In general, at the level of the random-phase approximation treatment, the superconducting transition temperature T_c decreases in stoichiometric bulk systems from the bilayer $\text{La}_3\text{Ni}_2\text{O}_7$ to the six-layer $\text{La}_7\text{Ni}_6\text{O}_{19}$, despite the m -dependent dominant pairing. Both in-plane and out-of-plane magnetic correlations are found to be quite complex. Within the in-plane direction, we obtained the peak of the magnetic susceptibility at $\mathbf{q} = (0.6\pi, 0.6\pi)$ for $\text{La}_5\text{Ni}_4\text{O}_{13}$ ($m = 4$) and $\text{La}_7\text{Ni}_6\text{O}_{19}$ ($m = 6$) and at $\mathbf{q} = (0.7\pi, 0.7\pi)$ for $\text{La}_6\text{Ni}_5\text{O}_{16}$ ($m = 5$). Along the out-of-plane direction, four layers are coupled as $\downarrow - \uparrow - \uparrow - \downarrow$ in $\text{La}_5\text{Ni}_4\text{O}_{13}$, five layers are coupled as $\uparrow - \uparrow - \downarrow - \uparrow - \uparrow$ in $\text{La}_6\text{Ni}_5\text{O}_{16}$, and six layers are coupled as $\uparrow - \downarrow - \downarrow - \uparrow - \uparrow - \downarrow$ in $\text{La}_7\text{Ni}_6\text{O}_{19}$.

DOI: [10.1103/h9kq-chh7](https://doi.org/10.1103/h9kq-chh7)

I. INTRODUCTION

The discovery of superconductivity in infinite-layer Sr-doped NdNiO_2 (d^9 configuration) films with a T_c of ~ 15 K [1] started the nickel era of unconventional high-temperature superconductivity [2–9], which are reminiscent of the successful stories of the cuprates [10–12] and iron-based superconductors [13,14]. Following the study of infinite-layer nickelates, other NiO_2 layered materials were found to superconduct, such as quintuple square-planar layered $\text{Nd}_6\text{Ni}_5\text{O}_{12}$ ($d^{8,8}$ configuration) with $T_c \sim 13$ K [15]. Because their electron configuration is close to d^9 , isoelectronic with Cu^{2+} , these nickelates are expected to have a $d_{x^2-y^2}$ -wave superconducting instability [16,17] as in the cuprates [11,12]. However, many theoretical and experimental efforts revealed

fundamental differences between square-planar layered nickelates and cuprates [6,18–23]. Very recently, pressure studies found superconductivity in bilayer $\text{La}_3\text{Ni}_2\text{O}_7$ [24] and trilayer $\text{La}_4\text{Ni}_3\text{O}_{10}$ [25,26] nickelates with corner-shared NiO_6 octahedra layers. This rapidly developing new avenue for the study of nickelate superconductors has already attracted much attention in condensed-matter physics and material sciences [27–44].

$\text{La}_3\text{Ni}_2\text{O}_7$ and $\text{La}_4\text{Ni}_3\text{O}_{10}$ belong to the Ruddlesden-Popper (RP) perovskite family $\text{La}_{m+1}\text{Ni}_m\text{O}_{3m+1}$ ($m = 1$ to ∞) involving bilayer and trilayer blocks stacking structures, respectively, as displayed in Fig. 1. In contrast to the square-planar layered nickelates $\text{La}_{m+1}\text{Ni}_m\text{O}_{2m+2}$ ($m = 1$ to ∞) [45–47], there are apical oxygens connecting the Ni layers in the RP nickelate family $\text{La}_{m+1}\text{Ni}_m\text{O}_{3m+1}$ ($m = 1$ to ∞). At ambient pressure, bilayer $\text{La}_3\text{Ni}_2\text{O}_7$ has an Amam (No. 63) structure [48], and thus, the NiO_6 octahedra are distorted. By applying hydrostatic pressure, the distortion of NiO_6 octahedra is suppressed around 14 GPa [28], accompanied by a first-order structural phase transition, resulting in an Fmmm

*Contact author: lflin@utk.edu

†Contact author: maierta@ornl.gov

‡Contact author: edagotto@utk.edu

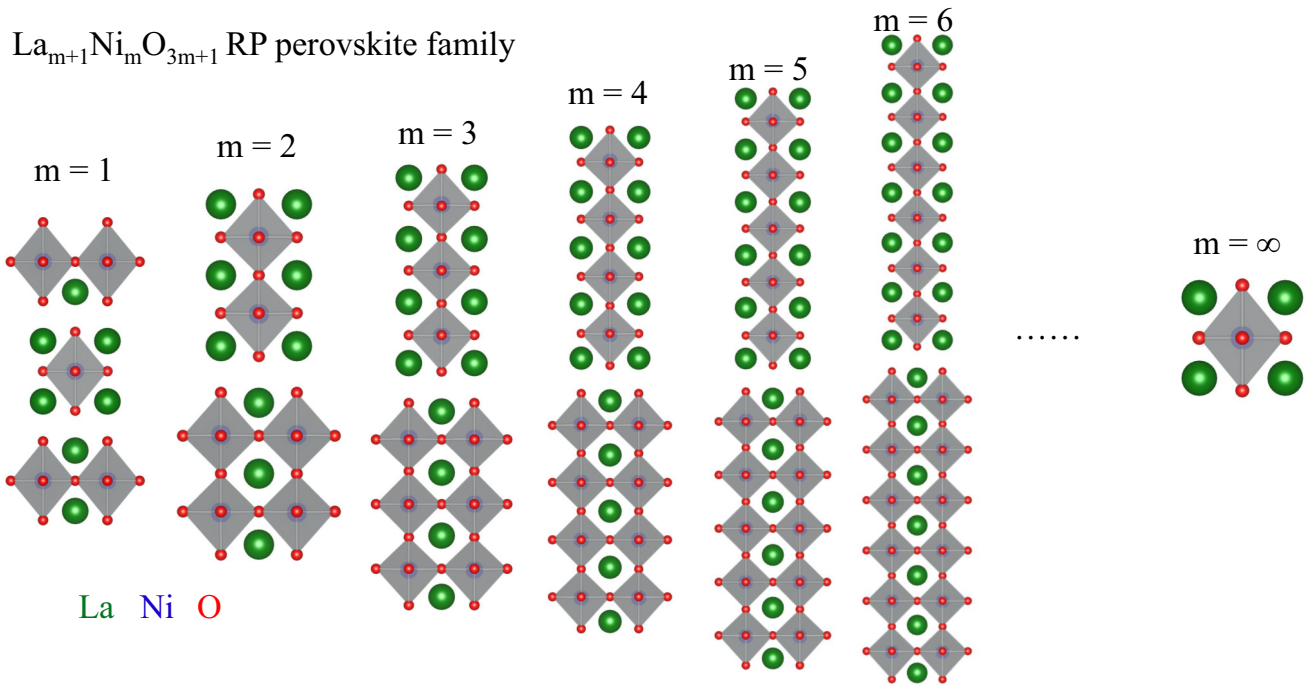


FIG. 1. Schematic crystal structures of the RP perovskite family $\text{La}_{m+1}\text{Ni}_m\text{O}_{3m+1}$ (green = La; blue = Ni; red = O). The visualization code VESTA is used [110].

(No. 69) phase without a tilting distortion of the NiO_6 octahedra [24]. By further increasing pressure, a superconducting state appears in a very broad pressure regime [24,49]. The initial claim of superconductivity in the $\text{La}_3\text{Ni}_2\text{O}_7$ system was based on measurements of the resistance by a four-terminal device, where the presence of zero resistance and the Meissner effect [24] was deduced by observing a sharp transition and a flat stage in resistance when using potassium bromide as the pressure-transmitting medium and a diamagnetic response in the susceptibility. Later, actual zero resistance [28,29,50] and Meissner effect [49] were observed by several groups, establishing the superconducting state in bilayer $\text{La}_3\text{Ni}_2\text{O}_7$. The superconducting volume fraction was reported to be around 48% in their high-quality superconducting samples by using the alternating-current magnetic susceptibility [49]. Very recently, a tetragonal $I4/mmm$ (No. 139) phase was proposed to be the correct high-pressure structure of $\text{La}_3\text{Ni}_2\text{O}_7$ from both theory [51] and experiment [52], instead of the $Fm\bar{3}m$ symmetry. The tilting distortion of the NiO_6 octahedra is suppressed in both phases. Due to the very small distortion from $I4/mmm$ (No. 139) to $Fm\bar{3}m$ (No. 69) in $\text{La}_3\text{Ni}_2\text{O}_7$ [53], those two phases are expected to display no fundamental differences, providing the same physics [54].

As in the bilayer $\text{La}_3\text{Ni}_2\text{O}_7$, the NiO_6 octahedra are also distorted in the trilayer nickelate $\text{La}_4\text{Ni}_3\text{O}_{10}$ with a $P21/c$ (No. 14) phase [55–59] at ambient pressure. Under hydrostatic pressure, the distortion of the NiO_6 octahedra is suppressed, and a high-symmetry $I4/mmm$ phase appears at around 15 GPa [25,26,60], once again without the tilting of oxygen octahedra. Following this structural transition, the superconducting state was also observed in a broad pressure range with a T_c of about 20–30 K [25,26,33,61], which is lower than in the bilayer $\text{La}_3\text{Ni}_2\text{O}_7$ [24]. The Meissner effect was

also observed in alternating-current magnetic susceptibility experiments with superconducting volume fraction around $\sim 80\%$ [26]. However, the single-layer RP nickelate La_2NiO_4 (see Fig. 1) has never been reported to superconduct at both ambient conditions and high pressure [50].

Theoretical studies have played a crucial role in providing insights into the nature of superconducting states in nickelates [62–94]. Density functional theory (DFT) calculations suggest that both $\text{La}_3\text{Ni}_2\text{O}_7$ and $\text{La}_4\text{Ni}_3\text{O}_{10}$ nickelates systems can be described using a two- e_g -orbital model in a bilayer or in a trilayer Ni lattice [33,95–97]. It is also indicated that the Fermi surfaces are contributed by Ni $d_{x^2-y^2}$ and $d_{3z^2-r^2}$ orbitals [56,95–98], with two-electron sheets with mixed e_g orbitals and a small hole pocket from the Ni $d_{3z^2-r^2}$ orbital at high pressure which is absent at ambient pressure. Angle-resolved photoemission spectroscopy experiments confirmed the Fermi surface obtained by DFT calculations for both $\text{La}_3\text{Ni}_2\text{O}_7$ and $\text{La}_4\text{Ni}_3\text{O}_{10}$ at ambient pressure [30,56].

Based on the two- e_g -orbitals model, theoretical studies suggested that s^\pm -wave pairing is dominant in bilayer $\text{La}_3\text{Ni}_2\text{O}_7$, induced by spin fluctuations due to the partial nesting of the Fermi surfaces with wave vectors approximately $(\pi, 0)$ or $(0, \pi)$ [62,64,66,69,99–101]. The s^\pm -wave pairing channel is believed to be driven mainly by strong interlayer coupling via the $d_{3z^2-r^2}$ orbital, but the $d_{x^2-y^2}$ orbital also contributes to the superconducting gap functions, comparable in some cases to the contributions of the $d_{3z^2-r^2}$ orbital [75,101]. Alternatively, there also appeared other theoretical studies, suggesting a dominant $d_{x^2-y^2}$ -wave or d_{xy} -wave superconducting pairing channel driven by the intralayer coupling [71,73,102,103]. In fact, the interplay between the intralayer and the interlayer pairing tendency was discussed many years ago by using $t - J$ models, where a prevailing interlayer

coupling leads to s -wave pairing while a prevailing stronger intralayer coupling results in d -wave pairing [104].

Considering these established results for bilayer $\text{La}_3\text{Ni}_2\text{O}_7$ and trilayer $\text{La}_4\text{Ni}_3\text{O}_{10}$, it is natural to wonder about the properties of other members of the RP nickelates family $\text{La}_{m+1}\text{Ni}_m\text{O}_{3m+1}$: Could the RP higher-order $m = 4$ –6 stacking nickelate be superconducting under pressure? In this case, what trends of superconductivity dominate in $\text{La}_{m+1}\text{Ni}_m\text{O}_{3m+1}$? What is the dependence of the pairing channel under pressure in $\text{La}_{m+1}\text{Ni}_m\text{O}_{3m+1}$? What are the magnetic correlations in $\text{La}_{m+1}\text{Ni}_m\text{O}_{3m+1}$? Could we establish a general intuitive picture of the RP nickelates systems?

To address these questions, here we theoretically study the high-symmetry I4/mmm phase of RP nickelates $\text{La}_{m+1}\text{Ni}_m\text{O}_{3m+1}$ ($m = 1$ to 6) without the tilting of the NiO_6 octahedra under pressure by using first-principles DFT and random-phase approximation (RPA) calculations. Our studies find many similarities but also some differences in the RP nickelates with different m -layer blocks. The $d_{3z^2-r^2}$ orbital displays the bonding-antibonding, or the bonding-antibonding-nonbonding splitting character, depending on the even or odd number of stacking layers m . In addition, the in-plane ratio of the interorbital hopping between the e_g orbitals and intraorbital hopping between $d_{x^2-y^2}$ orbitals was found to be large in $\text{La}_{m+1}\text{Ni}_m\text{O}_{3m+1}$, and this ratio increases from $m = 1$ to $m = 6$. In contrast to the s^\pm -wave pairing driven by spin fluctuations in the bilayer $\text{La}_3\text{Ni}_2\text{O}_7$ and trilayer $\text{La}_4\text{Ni}_3\text{O}_{10}$, two nearly degenerate $d_{x^2-y^2}$ -wave and s^\pm -wave instabilities are obtained in $\text{La}_5\text{Ni}_4\text{O}_{13}$ and $\text{La}_6\text{Ni}_5\text{O}_{16}$, while a leading s^\pm -wave state was found in $\text{La}_7\text{Ni}_6\text{O}_{19}$, with slightly higher calculated pairing strength λ than that of the $d_{x^2-y^2}$ -wave state. In general, at the level of the RPA treatment, the superconducting transition temperature T_c was expected to decrease in stoichiometric bulk systems from the bilayer $\text{La}_3\text{Ni}_2\text{O}_7$ to the six-layer $\text{La}_7\text{Ni}_6\text{O}_{19}$. Moreover, in the Ni planes, we obtained the peak of the magnetic susceptibility at $\mathbf{q} = (0.6\pi, 0.6\pi)$ for $\text{La}_5\text{Ni}_4\text{O}_{13}$ and $\text{La}_7\text{Ni}_6\text{O}_{19}$, and at $\mathbf{q} = (0.7\pi, 0.7\pi)$ for $\text{La}_6\text{Ni}_5\text{O}_{16}$. Furthermore, the out-of-plane magnetic correlations are complex in $\text{La}_{m+1}\text{Ni}_m\text{O}_{3m+1}$, with details depending on the stacking layer number m .

The scope of this work is to explore and understand the trends in the RP nickelates family $\text{La}_{m+1}\text{Ni}_m\text{O}_{3m+1}$ with different m -layer stacking. Considering previous studies of superconductivity in the bilayer $\text{La}_3\text{Ni}_2\text{O}_7$ and trilayer $\text{La}_4\text{Ni}_3\text{O}_{10}$, here we use the high-symmetry I4/mmm structure (see Fig. 1) without the tilting of NiO_6 octahedra to perform our study. The paper is organized as follows: In Sec. II the methods used are described, the results are presented in Secs. III and IV is devoted to the conclusions and discussions.

II. METHOD

In this work, first-principles DFT calculations were performed employing the Vienna *ab initio* simulation package (VASP) code by using the projector augmented wave method [105–107] with the generalized gradient approximation and the Perdew-Burke-Ernzerhof (PBE) exchange potential [108]. The plane-wave cutoff energy was set as 550 eV. Both lattice constants and atomic positions were fully relaxed until

the Hellman-Feynman force on each atom was smaller than 0.01 eV/Å. In addition, the \mathbf{k} -point mesh used was $20 \times 20 \times 2$ for the I4/mmm phase of $\text{La}_{m+1}\text{Ni}_m\text{O}_{3m+1}$ at 30 GPa.

To carry out further theoretical analyses, we derive maximally localized Wannier functions (MLWFs) projected on Ni 3d states using the WANNIER90 package [109] and construct low-energy e_g -orbital tight-binding models, consisting of orbital-dependent hopping matrices and crystal-field splittings. The resulting tight-binding Hamiltonian is expressed as

$$H_k = \sum_{\substack{i\gamma\gamma' \\ \bar{\alpha}\sigma}} t_{\gamma\gamma'}^{\bar{\alpha}} (c_{i\gamma\sigma}^\dagger c_{i+\bar{\alpha}\gamma'\sigma} + \text{H.c.}) + \sum_{i\gamma\sigma} \Delta_\gamma n_{i\gamma\sigma}. \quad (1)$$

The first term represents the hopping of an electron from orbital γ' at site $i + \bar{\alpha}$ to orbital γ at site i . $c_{i\gamma\sigma}^\dagger$ ($c_{i\gamma\sigma}$) is the creation (annihilation) operator of an electron at site i , orbital γ with spin σ . Δ_γ represents the crystal field of orbital γ with $n_{i\gamma\sigma} = c_{i\gamma\sigma}^\dagger c_{i\gamma\sigma}$. The vectors $\bar{\alpha}$ are along the three directions, defining different hopping neighbors. Here all hoppings involving Ni-Ni distances smaller than 10 Å are included in our calculations. In addition, the detailed input files of hopping matrices and crystal-field splittings can be found in a separate attachment in the Supplemental Material [111]. Based on the obtained Fermi energy for the stoichiometric ratio filling of $\text{La}_{m+1}\text{Ni}_m\text{O}_{3m+1}$ ($m = 1$ to 6) in our tight-binding model calculations, a 4001×4001 \mathbf{k} -mesh was used to calculate the Fermi surface.

To discuss the superconducting pairing and magnetic correlations in different m -layer stacking nickelates under pressure, here we used the many-body RPA method based on a perturbative weak-coupling expansion in the Hubbard interaction, similar to our previous analysis [62,97]. We considered a multiorbital Hubbard model, including the kinetic energy H_k and local interaction H_{int} terms. The model is written as $H = H_k + H_{\text{int}}$, where H_{int} includes the intraorbital Hubbard repulsion U , the interorbital Hubbard repulsion U' , the Hund's coupling J , and the interorbital electron-pair hopping J' , given by

$$H_{\text{int}} = U \sum_{i\gamma} n_{i\gamma\uparrow} n_{i\gamma\downarrow} + \left(U' - \frac{J}{2} \right) \sum_{\substack{i \\ \gamma < \gamma'}} n_{i\gamma} n_{i\gamma'} - 2J \sum_{\substack{i \\ \gamma < \gamma'}} \mathbf{S}_{i\gamma} \cdot \mathbf{S}_{i\gamma'} + J' \sum_{\substack{i \\ \gamma < \gamma'}} (P_{i\gamma}^\dagger P_{i\gamma'} + \text{H.c.}). \quad (2)$$

Here the standard relations $U' = U - 2J$ and $J' = J$ are assumed, with $n_{i\gamma} = n_{i\gamma\uparrow} + n_{i\gamma\downarrow}$ and $P_{i\gamma} = c_{i\gamma\downarrow} c_{i\gamma\uparrow}$.

In the multiorbital RPA approach [112–117], the spin susceptibility is obtained from the bare susceptibility (Lindhard function) $\chi_0(\mathbf{q})$ as $\chi(\mathbf{q}) = \chi_0(\mathbf{q})[1 - \mathcal{U}\chi_0(\mathbf{q})]^{-1}$. Here $\chi_0(\mathbf{q})$ is an orbital-dependent susceptibility tensor and \mathcal{U} is a tensor that contains the intraorbital U and interorbital U' density-density interactions, the Hund's rule coupling J , and the pair-hopping J' term. The pairing strength λ_α for channel α and the corresponding gap structure $g_\alpha(\mathbf{k})$ are obtained from solving an eigenvalue problem of the form

$$\int_{FS} d\mathbf{k}' \Gamma(\mathbf{k} - \mathbf{k}') g_\alpha(\mathbf{k}') = \lambda_\alpha g_\alpha(\mathbf{k}), \quad (3)$$

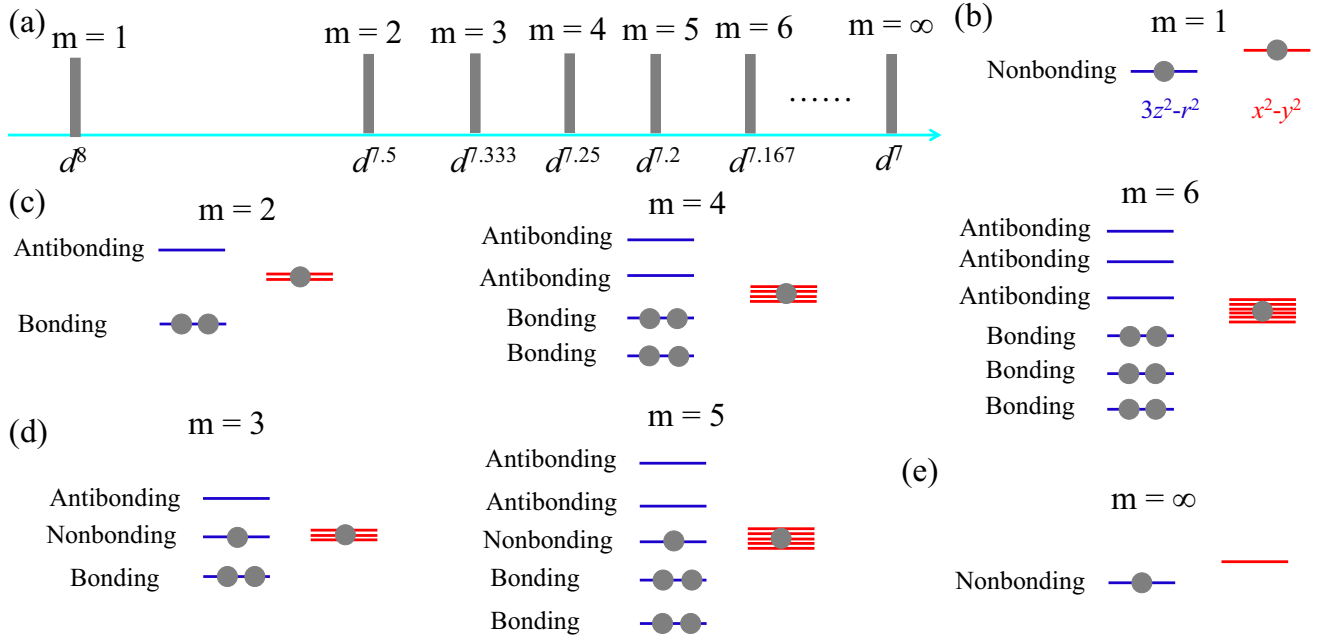


FIG. 2. (a) Schematic electronic densities of $3d$ electrons per Ni for different m -layer stacking RP nickelates $\text{La}_{m+1}\text{Ni}_m\text{O}_{3m+1}$. [(b)–(e)] Sketches of electronic states for two “active” e_g orbitals in $\text{La}_{m+1}\text{Ni}_m\text{O}_{3m+1}$ with layers (b) $m = 1$; (c) $m = 2, 4, 6$; and (d) $m = 3, 5$; and (e) ∞ , respectively. The light blue and pink horizontal lines represent $d_{3z^2-r^2}$ and $d_{x^2-y^2}$ states, respectively. The solid circles indicate the occupied electrons of e_g orbitals in the stoichiometric ratio $\text{La}_{m+1}\text{Ni}_m\text{O}_{3m+1}$.

where the momenta \mathbf{k} and \mathbf{k}' are on the Fermi surface FS and $\Gamma(\mathbf{k} - \mathbf{k}')$ contains the irreducible particle-particle vertex. While both spin and charge susceptibilities contribute to the pairing interaction, the dominant contribution comes from the RPA spin susceptibility tensor $\chi_{\ell_1 \ell_2 \ell_3 \ell_4}^s(\mathbf{k} - \mathbf{k}')$, where $\{\ell_i\}$ denote the different e_g orbitals of the RP nickelates, as shown in Fig. 1. For the electronic densities, we use the stoichiometric cases (i.e., 5 electrons for $m = 4$, corresponding to 1.25 electrons per site for the two e_g orbitals).

III. RESULTS

A. Model systems

RP nickelates $\text{La}_{m+1}\text{Ni}_m\text{O}_{3m+1}$ (m from 1 to ∞) have m -layer blocks of corner-shared NiO_6 octahedra. Considering the formal valence of La^{3+} and O^{2-} , the average valence of Ni in RP nickelates is given by $3 - 1/m$ as a function of m , leading to the $3d$ electron density n varying from 8 at $m = 1$ to 7 at $m = \infty$ as shown in Fig. 2(a). Since Ni t_{2g} orbitals are fully occupied, these nickelates could be regarded as “effective” two- e_g -orbital systems.

An important consequence of m -layer stacking in RP nickelates is the bonding-antibonding splitting of Ni $d_{3z^2-r^2}$ orbitals. Due to the single-layer blocks stacking, $d_{3z^2-r^2}$ orbitals do not have bonding-antibonding splitting in La_2NiO_4 ($m = 1$ case), as shown in Fig. 2(b). For the multiple layer stacking geometries in $\text{La}_{m+1}\text{Ni}_m\text{O}_{3m+1}$, the $d_{3z^2-r^2}$ orbital shows the bonding-antibonding, or the bonding-antibonding-nonbonding splitting, depending on the even or odd number of stacking layers. Similarly to the “dimer” physics in the $m = 2$ RP nickelate, the $m = 4$ and $m = 6$ compounds show an orbital-selective behavior [118,119], where the $d_{3z^2-r^2}$

orbital splits into bonding and antibonding states, while the $d_{x^2-y^2}$ orbital remains decoupled among planes, as shown in Fig. 2(c). Similarly to the “trimer” physics in the $m = 3$ RP nickelate, the $d_{3z^2-r^2}$ orbitals have bonding-antibonding and nonbonding splitting for $\text{La}_6\text{Ni}_5\text{O}_{16}$ ($m = 5$ case), as displayed in Fig. 2(d). At the other limit ($m = \infty$), i.e., the cubic perovskite LaNiO_3 , the $d_{3z^2-r^2}$ orbital does not have bonding-antibonding splitting as well [see Fig. 2(e)]. However, due to the strong in-plane hybridization between the e_g orbitals, both $d_{3z^2-r^2}$ and $d_{x^2-y^2}$ orbitals are not integer filled, leading to a “self-doping” effect in those two orbitals. Thus, this effect is also expected in all other m -layer stackings $\text{La}_{m+1}\text{Ni}_m\text{O}_{3m+1}$.

Note that the scope of this work is to explore and understand the trends in the RP nickelates family $\text{La}_{m+1}\text{Ni}_m\text{O}_{3m+1}$ with different m -layer stacking. Considering previous studies on the bilayer and trilayer nickelate bulk superconductors where superconductivity was found in the high-symmetry phase under pressure where the tilting of NiO_6 octahedra is absent, here we use the high-symmetry I4/mmm structure [47] (see Fig. 1) to mimic the uniform lattice structure expected for RP nickelates at 30 GPa. Since the electronic states near the Fermi level of RP nickelates $\text{La}_{m+1}\text{Ni}_m\text{O}_{3m+1}$ ($m = 1$ to 6) are mainly contributed by Ni $3d$ orbitals while the O $2p$ orbitals are located deeper in energy, a large charge-transfer gap between Ni $3d$ and O $2p$ states is expected as a common feature in these systems.

B. Tight-binding band structures and Fermi surfaces

To explore and understand the trends in the RP nickelates family with different m -layer stacking, we considered two e_g -orbitals for each m -layer system, i.e., the model has $2m$ bands. Based on the optimized crystal structures at

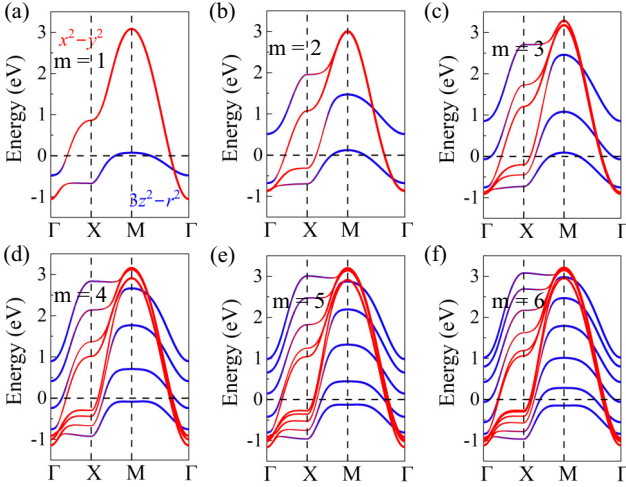


FIG. 3. Band structures of the tight-binding models for $\text{La}_{m+1}\text{Ni}_m\text{O}_{3m+1}$ ($m = 1$ to 6) at 30 GPa. The coordinates of the high-symmetry points in the Brillouin zone are $\Gamma = (0, 0, 0)$, $X = (0, 0.5, 0)$, and $M = (0.5, 0.5, 0)$. Here two e_g orbitals were considered in the tight-binding models with an overall filling of $n = 2$ to 7 for $m = 1$ to 6 (e.g., 1.2 electrons per site for $m = 5$).

30 GPa, we obtained hoppings and crystal-field splittings by using the MLWFs method in the WANNIER90 packages [109], and constructed an e_g -orbital tight-binding model for $\text{La}_{m+1}\text{Ni}_m\text{O}_{3m+1}$ ($m = 1$ to 6).

In Fig. 3, we plot the tight-binding band structures of the $I4/mmm$ phase for different m -layer stacking at 30 GPa. By increasing m from 1 to 6, the bandwidth of e_g orbitals is slightly increased by about 3%. In bilayer $\text{La}_3\text{Ni}_2\text{O}_7$ and trilayer $\text{La}_4\text{Ni}_3\text{O}_{10}$, a small hole pocket was found at the M point due to the bonding $d_{3z^2-r^2}$ orbitals. Note that this small γ hole pocket is not observed in the angle-resolved photoemission spectroscopy experiments for both bilayer and trilayer bulk systems at ambient pressure [30,56,61]. Due to the limitations of the high-pressure experiments, it is still very challenging to fully confirm the theoretical prediction for the high-pressure electronic structure of bilayer and trilayer nickelate systems. However, this small pocket was recently observed in the superconducting bilayer $(\text{La},\text{Pr})_3\text{Ni}_2\text{O}_7$ film grown on the a SrLaAlO_4 substrate [120]. Thus, the small γ pocket from the bonding state of the $d_{3z^2-r^2}$ orbitals may also be observed in the trilayer nickelate film as well, which deserves further experimental and theoretical work to explore. Such a small hole pocket is absent in $\text{La}_{m+1}\text{Ni}_m\text{O}_{3m+1}$ with $m = 4$ to 6, because the lowest bonding $d_{3z^2-r^2}$ orbital does not touch the Fermi level. Instead, the second lowest bonding state of $d_{3z^2-r^2}$ orbitals contribute to the γ sheets (γ_4 , γ_5 , and γ_6) in the Fermi level for the high-order RP nickelate $\text{La}_{m+1}\text{Ni}_m\text{O}_{3m+1}$ with $m = 4$ to 6.

Figure 4 summarizes the Fermi surfaces of RP nickelates. As shown in Fig. 4(a), there are two bands crossing the Fermi level in the single-layer La_2NiO_4 at 30 GPa, leading to an electronic sheet made of the mixed $d_{3z^2-r^2}$ and $d_{x^2-y^2}$ orbitals and a hole sheet originating from the $d_{3z^2-r^2}$ orbital. As mentioned above, $\text{La}_3\text{Ni}_2\text{O}_7$ and $\text{La}_4\text{Ni}_3\text{O}_{10}$ have small hole pockets around the M point [see Figs. 4(b) and 4(c)], and such a hole pocket is missing in $\text{La}_{m+1}\text{Ni}_m\text{O}_{3m+1}$ ($m = 4$ to 6)

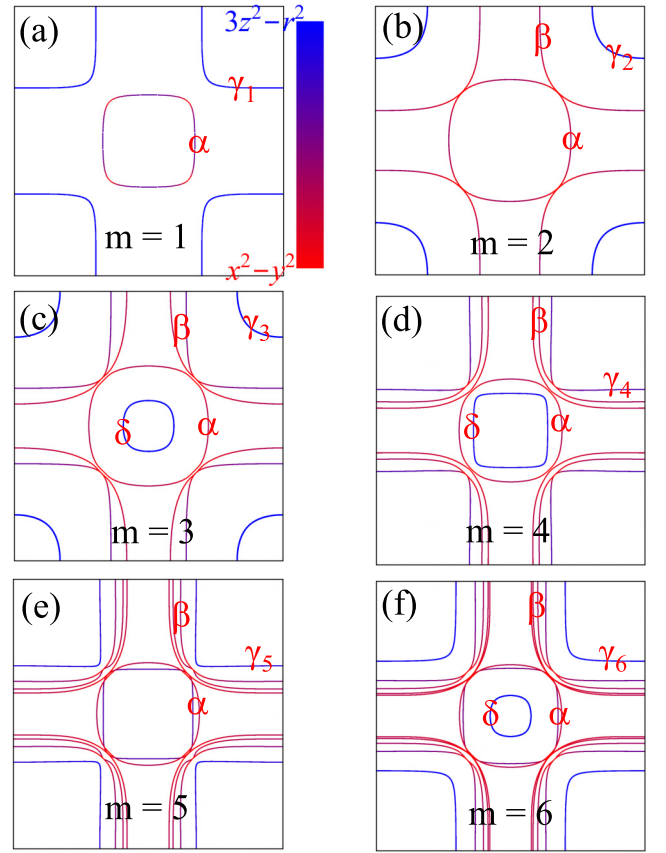


FIG. 4. Fermi surfaces of the tight-binding models for $\text{La}_{m+1}\text{Ni}_m\text{O}_{3m+1}$ ($m = 1$ to 6) at 30 GPa. Here two e_g orbitals were considered in the tight-binding models with an overall filling of $n = 2$ to 7 for $m = 1$ to 6 (e.g., 1.2 electrons per site for $m = 5$).

at 30 GPa as displayed in Figs. 4(d)–4(f). Some calculations did not observe the δ pocket in the $I4/mmm$ phase under high pressure [121], and this difference may be caused by the crystal structures of the different pressures used. In addition, a hole sheet from the $d_{3z^2-r^2}$ orbital was found near the M point in $\text{La}_6\text{Ni}_5\text{O}_{16}$ [see γ_5 in Fig. 4(e)] and $\text{La}_7\text{Ni}_6\text{O}_{19}$ [see γ_6 in Fig. 4(f)]. Similarly to the trilayer $\text{La}_4\text{Ni}_3\text{O}_{10}$ case [97], an electron δ pocket made up of a $d_{3z^2-r^2}$ orbital was also obtained in $\text{La}_7\text{Ni}_6\text{O}_{19}$, as in Fig. 4(f). The tight-binding Fermi surfaces of the $m = 4$ to $m = 6$ cases under pressure discussed here are also in agreement with previous DFT calculations in the tetragonal $I4/mmm$ phase of high-order RP nickelates without pressure [47].

We also notice the characteristic trend of hopping intensities. In the single-layer La_2NiO_4 (~ 0.333) at 30 GPa, the in-plane hybridization ($t_{x/y}^{12}/t_{x/y}^{22}$) between the $d_{3z^2-r^2}$ and $d_{x^2-y^2}$ orbitals is significantly small, compared to the bilayer and trilayer nickelates (~ 0.475 for $\text{La}_3\text{Ni}_2\text{O}_7$ and $\sim 0.532/0.543$ for $\text{La}_4\text{Ni}_3\text{O}_{10}$) [62,97]. This value $t_{x/y}^{12}/t_{x/y}^{22}$ continues to increase with the increase of high-order layer stacking at 30 GPa: $\sim 0.543/0.564$ for $\text{La}_5\text{Ni}_4\text{O}_{13}$, $\sim 0.545/0.573/0.580$ for $\text{La}_6\text{Ni}_5\text{O}_{16}$, and $\sim 0.544/0.568/0.584$ for $\text{La}_7\text{Ni}_6\text{O}_{19}$, suggesting that the in-plane hybridization between the $d_{3z^2-r^2}$ and $d_{x^2-y^2}$ orbitals and the layer number m has a positive correlation.

C. Superconducting pairing tendency

Next, we study the superconducting pairing tendencies in the RP nickelates. Here we carry out the RPA technique to investigate the pairing instability of the multi-orbital Hubbard model, $H = H_k + H_{\text{int}}$, where H_k is the single-particle part of the Hamiltonian with hopping matrix and crystal-field splittings from the I4/mmm phase of $\text{La}_{m+1}\text{Ni}_m\text{O}_{3m+1}$ at 30 GPa, given by Eq. (1). The RPA calculations of the pairing vertex are based on a perturbative weak-coupling expansion with respect to the electron-electron interaction part of the Hamiltonian (see the Methods section), H_{int} , given by Eq. (2), where the local Coulomb interaction matrix involves the intraorbital (U), interorbital (U'), Hund's rule coupling (J), and pair-hopping (J') terms [112–115].

For the single-layer $m = 1$ case, we do obtain a leading d_{xy} solution with a finite pairing eigenvalue at very small U based on the hopping and crystal-field splitting obtained under pressure. Beyond a critical U ($U > 0.4$ eV), we found a strong spin-density-wave instability around $(0, \pi)$ or $(\pi, 0)$ due to the perfect nesting between two γ_1 pockets. This suggests the superconducting pairing tendency is quite weak for the stoichiometric La_2NiO_4 case.

As discussed in previous work, the bilayer $\text{La}_3\text{Ni}_2\text{O}_7$ [62] and trilayer $\text{La}_4\text{Ni}_3\text{O}_{10}$ [97] have leading s^\pm -wave pairing instabilities driven by spin-fluctuations with different nesting vectors: $\mathbf{q} = (\pi, 0)$ or $(0, \pi)$ for $\text{La}_3\text{Ni}_2\text{O}_7$ and $\mathbf{q} = (\pi, \pi)$ for $\text{La}_4\text{Ni}_3\text{O}_{10}$. Furthermore, the s^\pm -wave pairing channel is more dominant than the $d_{x^2-y^2}$ channel [62,97,122]. This is supported by recent scanning tunneling microscopy experiments [123], where they found a much larger s -wave superconducting gap (~ 19 meV) than d -wave superconducting gap (~ 6 meV). For the high-order nickelates ($m = 4-6$), starting from the high-symmetry I4/mmm phase obtained from the previous study [47], we fully relaxed the atomic positions and lattice constants at 30 GPa. In the following, we focus on $\text{La}_{m+1}\text{Ni}_m\text{O}_{3m+1}$ with $m = 4$ to 6 and explore their superconducting pairing tendencies. As discussed in prior work [102], including long-range hoppings can qualitatively alter the RPA pairing susceptibilities. Here all hopping with Ni-Ni distances smaller than 10 Å are considered in our calculations.

Figure 5 shows our numerical results for the leading pairing instability in the high-order stacking $\text{La}_{m+1}\text{Ni}_m\text{O}_{3m+1}$ ($m = 4$ to 6), obtained by solving the eigenvalue problem in Eq. (3). Here we used Coulomb parameters $U = 1.4$ eV, $U' = U/2$, and $J = J' = U/4$, and the calculation was performed at a temperature $T = 0.01$ eV.

For the four-layer $m = 4$ case, we find nearly degenerate $d_{x^2-y^2}$ -wave and s^\pm -wave leading states with almost identical eigenvalues $\lambda_d = 0.1114$ and $\lambda_s = 0.1113$, respectively. For both the $d_{x^2-y^2}$ -wave and the s^\pm states, the gap is largest on the inner δ pocket and the γ_4 sheet with $d_{3z^2-r^2}$ character [see Fig. 5(a)]. For the s^\pm -wave state, the phase of the gap changes signs between these two sheets. The five-layer $m = 5$ case also has nearly degenerate $d_{x^2-y^2}$ -wave and s^\pm -wave leading solutions with similar pairing strengths, $\lambda_d = 0.1089$ and $\lambda_s = 0.101$, respectively. Here the gap is largest on the inner square-like sheet around Γ point and the γ_5 sheet with $d_{3z^2-r^2}$ character. The sign changes in or between these two sheets, as displayed in Fig. 5(b).

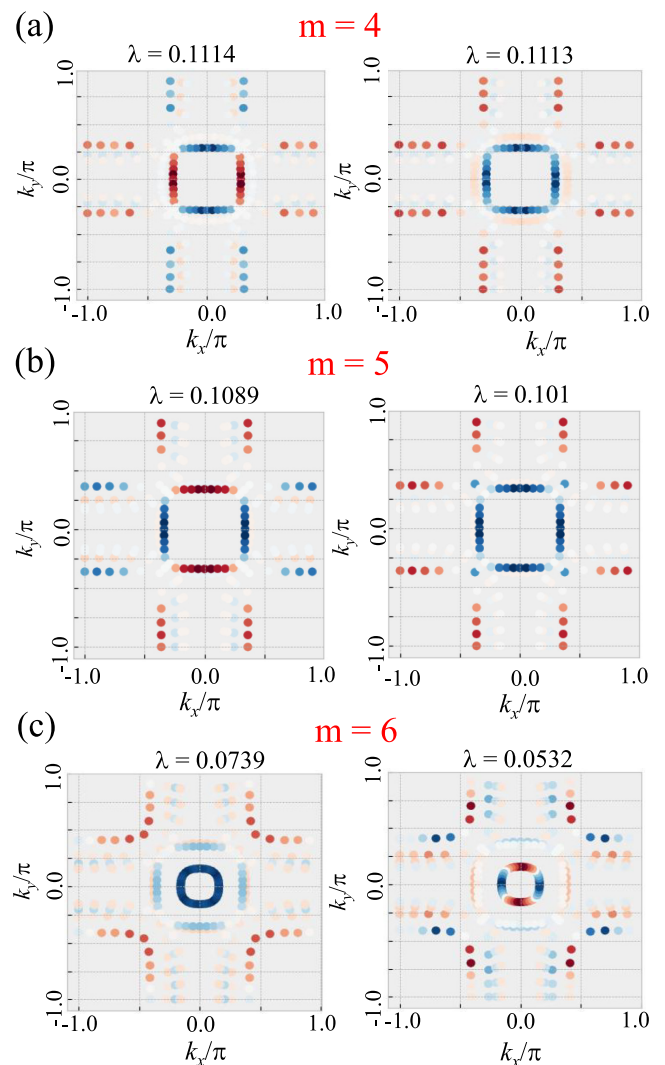


FIG. 5. The RPA calculated leading superconducting singlet gap structures $g_\alpha(\mathbf{k})$ for momenta \mathbf{k} on the Fermi surfaces for (a) $\text{La}_5\text{Ni}_4\text{O}_{13}$, (b) $\text{La}_6\text{Ni}_5\text{O}_{16}$, and (c) $\text{La}_7\text{Ni}_6\text{O}_{19}$ with corresponding pairing strengths λ at 30 GPa. The sign of $g_\alpha(\mathbf{k})$ is indicated by the color (red = positive, blue = negative), and its amplitude by the color darkness. We used Coulomb parameters $U = 1.4$ eV, $U' = U/2$, and $J = J' = U/4$. The calculation was performed at $T = 0.01$ eV.

The six-layer $m = 6$ case shown in Fig. 5(c) has a slightly reduced λ for the leading s^\pm -wave state and an even lower λ for the $d_{x^2-y^2}$ -wave channel. For both these states, the gap is largest on the inner δ pocket and the inner γ_6 sheet. We note that, similar to the infinite layer nickelates [124], the high-order RP layered nickelates ($m = 4, 5$, and 6) have nearly degenerate s^\pm -wave and $d_{x^2-y^2}$ -wave channels with pairing strengths that are much closer than those in the bilayer and trilayer cases.

We also note that the leading pairing strength $\lambda_d = 0.1114$ for four-layer stacking $\text{La}_5\text{Ni}_4\text{O}_{13}$ at $U = 1.4$ eV is already much smaller than the pairing strength $\lambda_s = 0.202$ we obtained for the trilayer system $\text{La}_4\text{Ni}_3\text{O}_{10}$ at 30 GPa but with a smaller interaction strength $U = 0.95$ eV [62], suggesting that the pairing correlations in the trilayer stacking system are much stronger. Moreover,

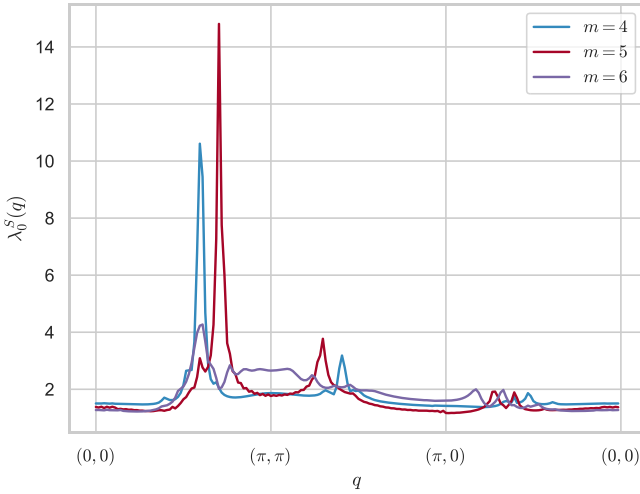


FIG. 6. The RPA calculated leading eigenvector $\lambda_0^S(\mathbf{q})$ of the spin-susceptibility matrix $\chi_{\ell_1\ell_1\ell_2\ell_2}$ for $\text{La}_5\text{Ni}_4\text{O}_{13}$ ($m = 4$), $\text{La}_6\text{Ni}_5\text{O}_{16}$ ($m = 5$), and $\text{La}_7\text{Ni}_6\text{O}_{19}$ ($m = 6$) for the I4/mmm phase at 30 GPa. The Coulomb parameters $U = 1.4$ eV, $U' = U/2$, and $J = J' = U/4$, and the calculation was performed for a temperature of $T = 0.01$ eV.

we found previously that the trilayer has smaller pairing strength than the bilayer 327-LNO at the same $U = 0.95$ ($\lambda_s \sim 0.39$). Since in our RPA treatment, the pairing strength λ enters exponentially in the equation for T_c , i.e., $T_c = \omega_0 e^{-1/\lambda}$ with a spin-fluctuation cut-off frequency ω_0 , this, and the new results in Fig. 5 suggests that T_c is expected to decrease in stoichiometric bulk systems as the layer stacking m increases. For the much lower pairing correlations in high-order cases ($m = 4, 5$, and 6), we can provide an intuitive understanding based on the electronic structures. Here the lowest bonding state of $d_{3z^2-r^2}$ orbitals does not touch the Fermi level in those high-order RP nickelates, leading to the absence of the small γ pocket around the M point. Instead, the γ sheets arise from the second lowest bonding state of $d_{3z^2-r^2}$ orbitals with large size shapes. Thus, the nesting is not perfect, and the Fermi velocities are also larger, compared to the bilayer and trilayer cases. Therefore, the pairing correlations become much weaker in the high-order RP nickelates, at least at the RPA level.

D. Magnetic correlations

Finally, we discuss the magnetic correlations in the RP nickelates $\text{La}_{m+1}\text{Ni}_m\text{O}_{3m+1}$ with different layer blocks m . To this end, we analyze the RPA enhanced spin susceptibility tensor $\chi(\mathbf{q}, \omega = 0)$ that is obtained from the Lindhart function tensor $\chi_0(\mathbf{q})$ as

$$\chi(\mathbf{q}) = \chi_0(\mathbf{q})[1 - \mathcal{U}\chi_0(\mathbf{q})]^{-1}, \quad (4)$$

where all the quantities are rank-four tensors in the orbital indices $\ell_1, \ell_2, \ell_3, \ell_4$ and \mathcal{U} is a tensor involving the interaction parameters [112]. The physical spin susceptibility is obtained by summing the pairwise diagonal tensor $\chi_{\ell_1\ell_1\ell_2\ell_2}(\mathbf{q})$ over ℓ_1, ℓ_2 . Here all the long-range hopping with the Ni-Ni distances smaller than 10 Å are considered in our calculations.

As displayed in Fig. 6, the leading eigenvalue $\lambda_0^S(\mathbf{q})$ of $\chi_{\ell_1\ell_1\ell_2\ell_2}(\mathbf{q})$ for momenta \mathbf{q} along a high-symmetry path in

the Brillouin zone has the strongest in-plane peak at $\mathbf{q} = (0.6\pi, 0.6\pi)$, $\mathbf{q} = (0.7\pi, 0.7\pi)$, and $\mathbf{q} = (0.6\pi, 0.6\pi)$ for $m = 4, 5$, and 6 , respectively. This is different from the bilayer and trilayer systems [62,97], for which we previously found that the in-plane peak is near $(\pi, 0)$ or $(0, \pi)$ and (π, π) , respectively. In the RPA treatment, this difference arises from differences in the Fermi surface and the respective nesting wave vectors. This may be a consequence of the intraorbital and interorbital hopping mechanisms with different electronic densities, as discussed in previous studies [125–127].

Our original expectation was that the magnetic behavior of even- and odd-layered RP phases would follow similar trends along the z axis. However, our results have revealed a more complex picture, where the interplay between inter-layer exchange, structural distortions, and symmetry effects appears to be more intricate than initially anticipated. Figure 7 shows the corresponding eigenvector $\varphi_0^S(\mathbf{q})$ at the in-plane \mathbf{q} for which its eigenvalue $\lambda_0^S(\mathbf{q})$ has a maximum. One sees that the main contributions to the magnetic correlations come from the $d_{3z^2-r^2}$ orbitals from outer Ni layers. In addition, the out-of-plane, interlayer magnetic correlations determined by the relative sign of the eigenvector contributions also strongly depend on the number of layers m . In the four- and five-layer systems, the outer Ni layers are coupled ferromagnetically, but in the six-layer system, they have antiferromagnetic coupling. For $\text{La}_5\text{Ni}_4\text{O}_{13}$, the four layers are coupled as $\downarrow - \uparrow - \uparrow - \downarrow$ and the five layers are coupled as $\uparrow - \uparrow - \downarrow - \uparrow - \uparrow$ along the out-of-plane directions, while the $\text{La}_7\text{Ni}_6\text{O}_{19}$ has an $\uparrow - \downarrow - \downarrow - \uparrow - \uparrow - \downarrow$ coupling. In contrast to the trilayer case, we do not find a spin-zero Ni layer in high-order $\text{La}_{m+1}\text{Ni}_m\text{O}_{3m+1}$ with $m = 4$ to 6 .

IV. CONCLUSIONS AND DISCUSSIONS

In this work, studying the high-symmetry I4/mmm phase under pressure, we systematically explored physical trends in the RP m -layer stacking nickelates $\text{La}_{m+1}\text{Ni}_m\text{O}_{3m+1}$. Near the Fermi surface, the states are mainly contributed by Ni $3d$ orbitals, because O $2p$ orbitals are located deeper in energy, suggesting a common picture in nickelate superconductors involving a large charge-transfer gap between $3d$ and $2p$ states. Furthermore, the $d_{3z^2-r^2}$ orbital exhibits the bonding-antibonding or the bonding-antibonding-nonbonding splitting characters, depending on whether m is even or odd. Due to the in-plane interorbital hopping between the $d_{3z^2-r^2}$ and $d_{x^2-y^2}$ orbitals, the electronic occupations of both orbitals is not an integer, leading to a “self-doping” situation, as observed in other RP nickelate superconductors. Furthermore, the ratio of the in-plane interorbital hopping between the e_g orbitals and in-plane intraorbital hopping between $d_{x^2-y^2}$ orbitals is found to increase with m .

For the single-layer $m = 1$ case, we found a strong spin-density-wave instability around $(\pi, 0)$ or $(0, \pi)$ due to the perfect nesting between two nearly flat γ_1 pockets. Previous studies found very interesting diagonal spin- and charge-stripes states in hole-doped $m = 1$ case [129,130]. We believe that the phase diagram should be very rich in this two-dimensional single-layer system with different electronic densities of e_g orbitals, similar to our previous work for the bilayer phase diagram under

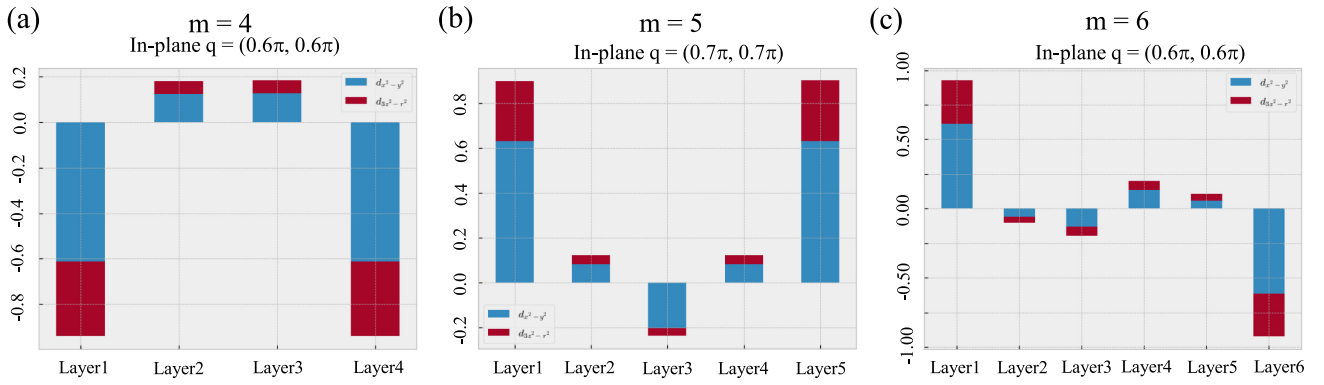


FIG. 7. Leading eigenvector of the susceptibility matrix $\chi_{\ell_1\ell_1,\ell_2\ell_2}(q, \omega = 0)$ at the in-plane q -vector for which its leading eigenvalue $\lambda_0^S(q)$ has a maximum, for (a) $\text{La}_5\text{Ni}_4\text{O}_{13}$, (b) $\text{La}_6\text{Ni}_5\text{O}_{16}$, and (c) $\text{La}_7\text{Ni}_6\text{O}_{19}$. The contributions of $d_{3z^2-r^2}$ and $d_{x^2-y^2}$ orbitals are shown by blue and red colors. The Coulomb parameters are $U = 1.4$ eV, $U' = U/2$, and $J = J' = U/4$, and the calculation was performed for temperature $T = 0.01$ eV.

doping [82]. This is caused by strong competition between antiferromagnetic and ferromagnetic tendencies varying doping, which is related to intraorbital and interorbital hoppings [125–127]. The magnetic phase diagram of the single-layer nickelate with varying doping is very interesting, as well as the pressure effect. Those deserve more careful and detailed studies, but they are beyond the current purpose of this work. Thus, we leave this doping and pressure effect in the interesting single-layer La_2NiO_4 to further work.

For the bilayer $m = 2$ and trilayer $m = 3$ cases [62,97], the spin-fluctuation-driven s^\pm -wave state is dominant in both cases. For $m = 4$ and $m = 5$ cases, we find two nearly degenerate $d_{x^2-y^2}$ -wave and s^\pm -wave leading states. However, in $\text{La}_7\text{Ni}_6\text{O}_{19}$, this six-layer stacking system has a slightly reduced λ for the leading s^\pm -wave state and a slight lower λ for the $d_{x^2-y^2}$ -wave channel. In general, at the level of the RPA treatment, *the superconducting transition temperature T_c decreases as the layer stacking number m increases in stoichiometric bulk systems.* Recently, some studies predicted that in the ideal situation, T_c may recover in the high-order RP nickelates, as compared to the trilayer $\text{La}_4\text{Ni}_3\text{O}_{10}$, due to spatial modulation of the interlayer pairing along the z axis [94,128]. This brings a very interesting question: whether or not T_c might be potentially enhanced by valence tuning, etc. In our previous work, the small γ from bonding state of the $d_{3z^2-r^2}$ orbitals was shown to be important for superconductivity in our previous work on bilayer and trilayer nickelates based on the same RPA framework [62,97]. By tuning the valence of Ni, corresponding to tuning the electronic doping, a small γ pocket from the lowest bonding state of $d_{3z^2-r^2}$ orbitals can be also obtained in high-order RP cases. Thus, in this framework it is possible to have a stronger pairing strength, a subject that deserves further investigations, which could be the next step for further work.

Similarly to the pairing instability, magnetic correlations are found to be quite complex in the RP nickelates, depending on the stacking layer number m . As mentioned above, single-layer La_2NiO_4 has a strong stripe instability characterized by $\mathbf{q} = (\pi, 0)$ or $(0, \pi)$, similar to our previous finding on bilayer $\text{La}_3\text{Ni}_2\text{O}_7$ [62]. For the trilayer $\text{La}_4\text{Ni}_3\text{O}_{10}$ [97], the

peak of the magnetic susceptibility was found at $\mathbf{q} = (\pi, \pi)$. For $\text{La}_5\text{Ni}_4\text{O}_{13}$ ($m = 4$) and $\text{La}_7\text{Ni}_6\text{O}_{19}$ ($m = 6$), the peak position is shifted to $\mathbf{q} \approx (0.6\pi, 0.6\pi)$, and for $\text{La}_6\text{Ni}_5\text{O}_{16}$ ($m = 5$) the peak position is at $\mathbf{q} \approx (0.7\pi, 0.7\pi)$. Moreover, the out-of-plane magnetic correlations strongly depend on the number of layers m .

As shown in Fig. 2, there is no bonding-antibonding state for the $d_{3z^2-r^2}$ orbitals for $m = 1$ and $m = \infty$ cases, but this splitting exists in other layered RP nickelates, suggesting the $d_{3z^2-r^2}$ orbital may play different roles in different compounds of the same family. As discussed in the context of bilayer and trilayer RP nickelates, the interlayer coupling is believed to be important for a variety of reasons [62,64,66,69,97,99–101]. A recent scanning tunneling microscopy experiment found a dominant interlayer superconducting gap in $\text{La}_2\text{PrNi}_2\text{O}_7$ thin films, where its magnitude is much larger than that of the intralayer gap [123]. In our present work, we also found that the interlayer coupling is important in those high-order RP nickelates. However, at $m = 1$ case, corresponding to the LaNiO_3 case with d^7 configuration, the superconductivity was believed to be driven by the intralayer $d_{x^2-y^2}$ orbital, similar to cuprates, as experimentally observed in the $\text{LaNiO}_3/\text{La}_{0.7}\text{Sr}_{0.3}\text{MnO}_3$ superlattice with $T_c \sim 2$ K [131] and theoretically predicted in $\text{LaNiO}_3/\text{LaMnO}_3$ superlattices [12]. In addition a recent theoretical work suggests a single-band d -wave superconductivity in single-layer La_2NiO_4 [132]. Thus, we believe that the RP nickelate family cannot be understood via a simple electronic filling context. To establish an uniform picture for the RP nickelate systems is very important and interesting, but still needs more comprehensive and detailed studies.

Figure 8 summarizes our findings. We hope that our comprehensive study of the m dependence of magnetic and pairing properties will stimulate experimental efforts to verify our theoretical predictions. As reported in Ref. [58], it is very challenging to prepare samples in bulk format since they are not thermodynamically stable under the high $p\text{O}_2$ crystal growth method. However, the thin film of high-order $\text{La}_{m+1}\text{Ni}_m\text{O}_{3m+1}$ ($m = 4$ and $m = 5$) [133] and $\text{Nd}_{m+1}\text{Ni}_m\text{O}_{3m+1}$ ($m = 4$ and $m = 5$) [134] has been stabi-

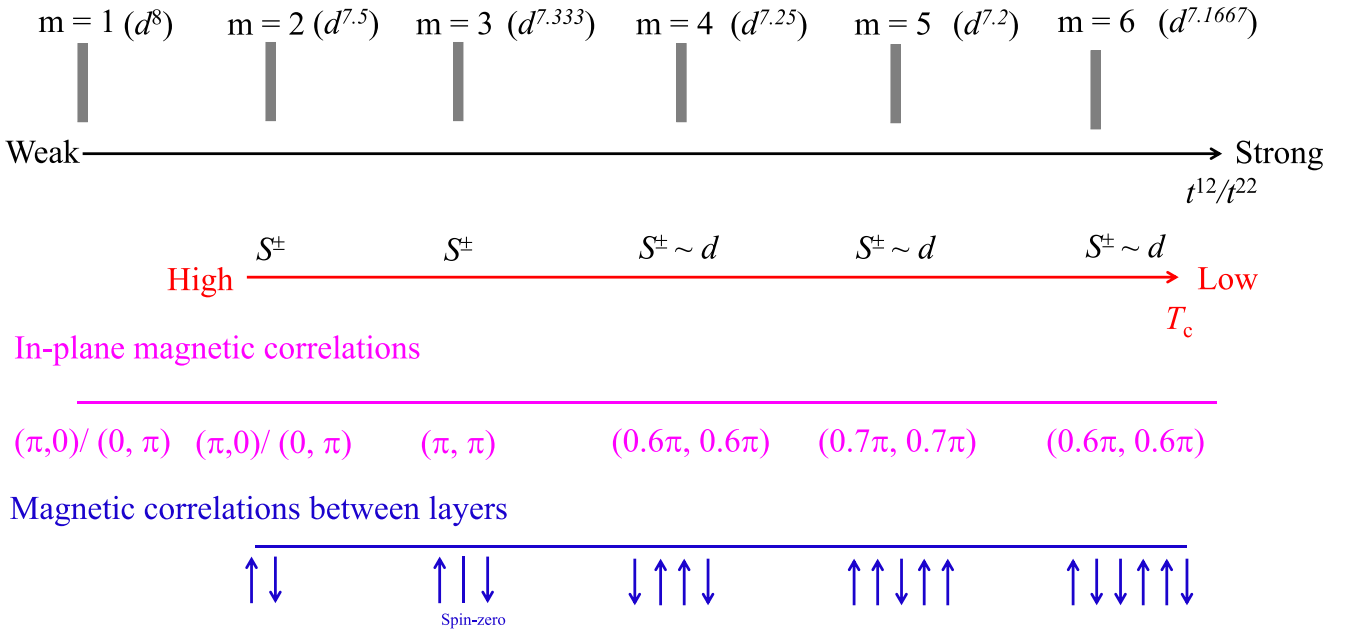


FIG. 8. Summary of our main findings for the I4/mmm phase of the $\text{La}_{m+1}\text{Ni}_m\text{O}_{3m+1}$ family with different layer stacking number m under pressure.

lized in experiments using reactive molecular-beam epitaxy. In this case, strain can be used to manipulate their electronic structures in the thin-film format of the high-order RP nickelates. Furthermore, the superconductivity temperature-pressure phase diagrams were also reported in the $\text{La}_3\text{Ni}_2\text{O}_7$ films on SrTiO_3 , NdGaO_3 , and LaAlO_3 substrates [135]. Moreover, the layered nickelate bulk can be prepared using the melt salt method, as reported in $\text{La}_5\text{Ni}_3\text{O}_{11}$ [136], which may provide a possible direction to grow the higher-order RP phases ($m = 4-6$) in bulk form. Thus, we believe our theoretical predictions, based on idealized bulk calculations under pressure, could provide a useful starting point or qualitative guidance for future experiments.

Very recently, Y.-F. Zhao *et al.* [137] found that tensile strain can induce a small γ pocket from the lowest bonding state of $d_{3z^2-r^2}$ orbitals near M points in the I4/mmm phase of four-layer stacking $\text{La}_5\text{Ni}_4\text{O}_{13}$ and five-layer stacking $\text{La}_6\text{Ni}_5\text{O}_{16}$, while a compressive strain cannot induce this pocket for both cases, suggesting that the pressure may not induce the γ pocket as well. In the previous context of bilayer and trilayer nickelates, this pocket is believed to be crucial for superconductivity. Thus, the next step is to investigate in the high-order stacking nickelates $\text{La}_{m+1}\text{Ni}_m\text{O}_{3m+1}$ ($m = 4$ to 6) the connection between superconductivity and the hole pocket from the lowest bonding state of $d_{3z^2-r^2}$ orbitals. Especially, to explore if the superconductivity can be enhanced in those high-order La-based systems or in other rare-earth RP nickelates ($m = 4-6$ case) when the small γ pocket from the lowest bonding state of $d_{3z^2-r^2}$ orbitals exists near the M point.

ACKNOWLEDGMENTS

This work was supported by the U.S. Department of Energy, Office of Science, Basic Energy Sciences, Materials Sciences and Engineering Division. This manuscript has been

authored by UT-Battelle, LLC, under contract DE-AC05-00OR22725 with the US Department of Energy (DOE). The US government retains and the publisher, by accepting the article for publication, acknowledges that the US government retains a nonexclusive, paid-up, irrevocable, worldwide license to publish or reproduce the published form of this manuscript, or allow others to do so, for US government purposes. DOE will provide public access to these results of federally sponsored research in accordance with the DOE Public Access Plan [138].

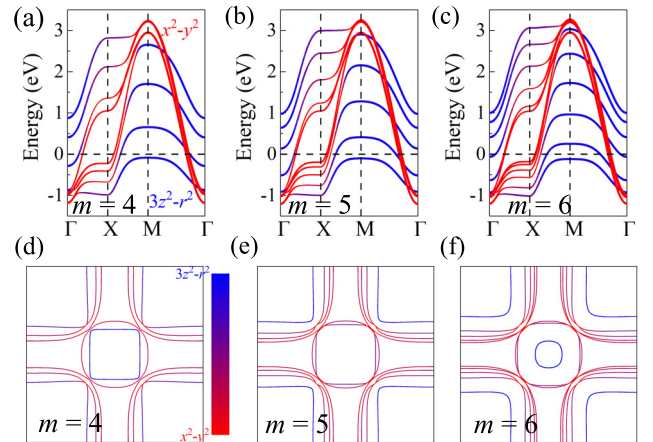


FIG. 9. [(a)–(c)] Band structures and [(d)–(f)] Fermi surfaces of the tight-binding models for $\text{La}_{m+1}\text{Ni}_m\text{O}_{3m+1}$ ($m = 3$ to 6) at 30 GPa. The coordinates of the high-symmetry points in the Brillouin zone are $\Gamma = (0, 0, 0)$, $X = (0, 0.5, 0)$, and $M = (0.5, 0.5, 0)$. Here two e_g orbitals were considered in the tight-binding models with an overall filling of $n = 5$ to 7 for $m = 4$ to 6 (e.g., 1.2 electrons per site for $m = 6$) with long-range hoppings up to the Ni-Ni distances 10 Å. Those hoppings are obtained from band structures of the DFT with $U_{\text{eff}} = 4$ eV.

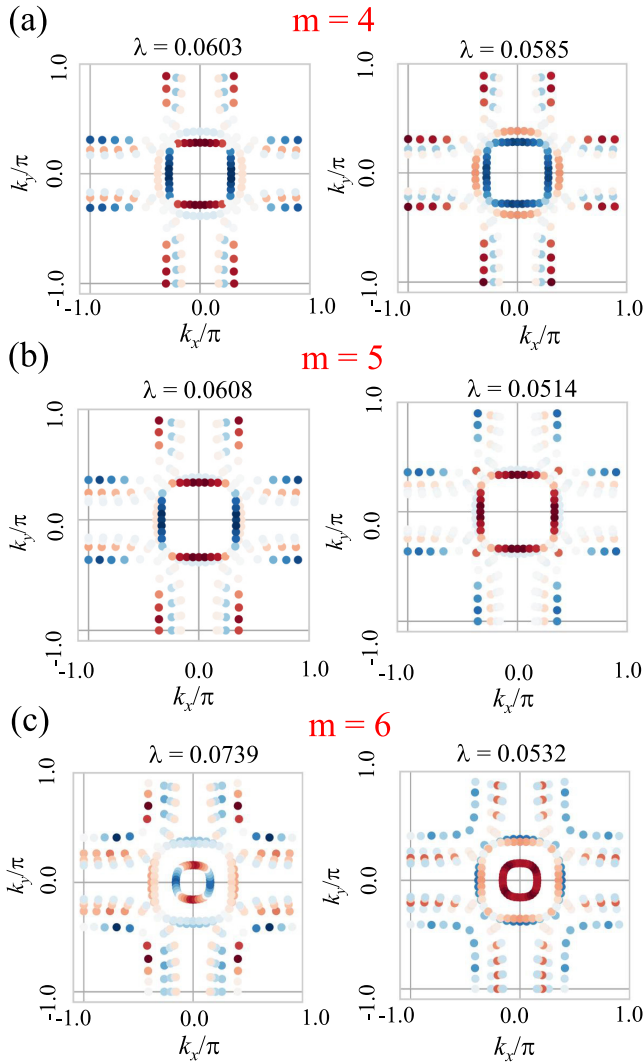


FIG. 10. The RPA calculated leading superconducting singlet gap structures $g_\alpha(\mathbf{k})$ for momenta \mathbf{k} on the Fermi surfaces for (a) $\text{La}_5\text{Ni}_4\text{O}_{13}$, (b) $\text{La}_6\text{Ni}_5\text{O}_{16}$, and (c) $\text{La}_7\text{Ni}_6\text{O}_{19}$ with corresponding pairing strengths λ at 30 GPa. The sign of $g_\alpha(\mathbf{k})$ is indicated by the color (red = positive, blue = negative), and its amplitude by the color darkness. We used Coulomb parameters $U = 1.4$ eV, $U' = 1.0$ eV, and $J = J' = 0.2$ eV. The calculation was performed at $T = 0.01$ eV.

DATA AVAILABILITY

The dataset of the main findings of this study is openly available in a Zenodo Repository [139]. In addition, the hopping and crystal-field parameters for our tight-binding and RPA calculations are available in a separate file of the Supplementary Material [111] and Zenodo Repository [139] for reproducing our results. Simulation RPA codes are available at [140].

APPENDIX

1. Electronic structures using hoppings obtained by DFT+ U

In addition, we also considered the Fermi surface topology varying the Hubbard interaction U . First, we calculated the electronic structures of the I4/mmm phase of the high-order ($m = 4-6$) RP layer nickelate at 30 GPa by introducing the local density approach (LDA) plus U using the Dudarev's rotationally invariant formulation [141] with $U_{\text{eff}} = 4$ eV, as used in previous studies of nickelates [24,62]. The e_g orbitals contribute the most to the low-energy physics near the Fermi level, similarly to the case without U discussed in the main text. However, the t_{2g} bands of those high-order cases shift away from the e_g state. Next, we studied the tight-binding band structures and Fermi surfaces including the longer-range hoppings with the Ni-Ni distances smaller than 10 Å by fitting Wannier bands with DFT+ U_{eff} ($U_{\text{eff}} = 4$ eV) band structures, as shown in Fig. 9. The projected band structures of the e_g states do not change much compared to the electronic structures at $U = 0$ eV discussed in the main text, where the lowest bonding band of the $d_{3z^2-r^2}$ orbitals does not touch the Fermi surface for all three cases.

2. Gap structures for smaller J_H

Furthermore, we also calculated the leading pairing instability in the high-order stacking $\text{La}_{m+1}\text{Ni}_m\text{O}_{3m+1}$ ($m = 4$ to 6) for smaller J_H , as shown in Fig. 10. Here, we used Coulomb parameters $U = 1.4$ eV, $U' = 1.0$ eV, and $J = J' = 0.2$ eV, and the calculation was performed at a temperature $T = 0.01$ eV. Similarly to the cases with the larger J_H , both the $d_{x^2-y^2}$ -wave and s^\pm -wave states are dominant solutions and have close eigenvalues λ 's, but the calculated values of λ 's are generally reduced.

[1] D. Li, K. Lee, B. Y. Wang, M. Osada, S. Crossley, H. R. Lee, Y. Cui, Yi, Y. Hikita, and H. Y. Hwang, Superconductivity in an infinite-layer nickelate, *Nature (London)* **572**, 624 (2019).
 [2] Y. Nomura, M. Hirayama, T. Tadano, Y. Yoshimoto, K. Nakamura, and R. Arita, Formation of a two-dimensional single-component correlated electron system and band engineering in the nickelate superconductor NdNiO_2 , *Phys. Rev. B* **100**, 205138 (2019).
 [3] A. S. Botana and M. R. Norman, Similarities and differences between LaNiO_2 and CaCuO_2 and implications for superconductivity, *Phys. Rev. X* **10**, 011024 (2020).
 [4] D. Li, B. Y. Wang, K. Lee, S. P. Harvey, M. Osada, B. H. Goodge, L. F. Kourkoutis, and H. Y. Hwang, Superconducting

dome in $\text{Nd}_{1-x}\text{Sr}_x\text{NiO}_2$ infinite layer films, *Phys. Rev. Lett.* **125**, 027001 (2020).

[5] Y. Nomura and R. Arita, Superconductivity in infinite-layer nickelates, *Rep. Prog. Phys.* **85**, 052501 (2022).
 [6] Y. Zhang, L.-F. Lin, W. Hu, A. Moreo, S. Dong, and E. Dagotto, Similarities and differences between nickelate and cuprate films grown on a SrTiO_3 substrate, *Phys. Rev. B* **102**, 195117 (2020).
 [7] S. W. Zeng, X. M. Yin, C. J. Li, L. E. Chow, C. S. Tang, K. Han, Z. Huang, Y. Cao, D. Y. Wan, Z. T. Zhang, Z. S. Lim, C. Z. Diao, P. Yang, A. T. S. Wee, S. J. Pennycook, and A. Ariando, Observation of perfect diamagnetism and interfacial effect on the electronic structures in

- infinite layer $\text{Nd}_{0.8}\text{Sr}_{0.2}\text{NiO}_2$ superconductors, *Nat. Commun.* **13**, 743 (2022).
- [8] C. Yang, R. A. Ortiz, Y. Wang, W. Sigle, H. Wang, E. Benckiser, B. Keimer, and P. A. V. Aken, Thickness-dependent interface polarity in infinite-layer nickelate superlattices, *Nano Lett.* **23**, 3291 (2023).
- [9] Q. Gu and W.-H. Wen, Superconductivity in nickel-based 112 systems, *Innovation* **3**, 100202 (2022).
- [10] J. G. Bednorz and K. A. Müller, Possible high- T_c superconductivity in the Ba-La-Cu-O system, *Z. Phys. B* **64**, 189 (1986).
- [11] E. Dagotto, Correlated electrons in high-temperature superconductors, *Rev. Mod. Phys.* **66**, 763 (1994).
- [12] J. Chaloupka and G. Khaliullin, Orbital order and possible superconductivity in $\text{LaNiO}_3/\text{LaMO}_3$ superlattices, *Phys. Rev. Lett.* **100**, 016404 (2008).
- [13] Y. Kamihara, T. Watanabe, M. Hirano, and H. Hosono, Iron-based layered superconductor $\text{La}[\text{O}_{1-x}\text{F}_x]\text{FeAs}$ ($x = 0.05 - 0.12$) with $T_c = 26$ K, *J. Am. Chem. Soc.* **130**, 3296 (2008).
- [14] E. Dagotto, *Colloquium: The unexpected properties of alkali metal iron selenide superconductors*, *Rev. Mod. Phys.* **85**, 849 (2013).
- [15] G. A. Pan, D. F. Segedin, H. LaBollita, Q. Song, E. M. Nica, B. H. Goodge, A. T. Pierce, S. Doyle, S. Novakov, D. C. Carrizales, A. T. N'Diaye, P. Shafer, H. Paik, J. T. Heron, J. A. Mason, A. Yacoby, L. F. Kourkoutis, O. Erten, C. M. Brooks, A. S. Botana, and J. A. Mundy, Superconductivity in a quintuple-layer square-planar nickelate, *Nat. Mater.* **21**, 160 (2022).
- [16] X. Wu, D. DiSante, T. Schwemmer, W. Hanke, H. Y. Hwang, S. Raghu, and R. Thomale, Robust $d_{x^2-y^2}$ -wave superconductivity of infinite-layer nickelates, *Phys. Rev. B* **101**, 060504(R) (2020).
- [17] H. Sakakibara, H. Usui, K. Suzuki, T. Kotani, H. Aoki, and K. Kuroki, Model construction and a possibility of cupratelike pairing in a new d^9 nickelate superconductor (Nd, Sr) NiO_2 , *Phys. Rev. Lett.* **125**, 077003 (2020).
- [18] M. Jiang, M. Berciu, and G. A. Sawatzky, Critical nature of the Ni spin state in doped NdNiO_2 , *Phys. Rev. Lett.* **124**, 207004 (2020).
- [19] P. Werner and S. Hoshino, Nickelate superconductors: Multi-orbital nature and spin freezing, *Phys. Rev. B* **101**, 041104(R) (2020).
- [20] Y. Gu, S. Zhu, X. Wang, J. Hu, and H. Chen, A substantial hybridization between correlated Ni-d orbital and itinerant electrons in infinite-layer nickelates, *Commun. Phys.* **3**, 84 (2020).
- [21] J. Karp, A. S. Botana, M. R. Norman, H. Park, M. Zingl, and A. Millis, Many-body electronic structure of NdNiO_2 and CaCuO_2 , *Phys. Rev. X* **10**, 021061 (2020).
- [22] J. Fowlie, M. Hadjimichael, M. M. Martins, D. Li, M. Osada, B. Y. Wang, K. Lee, Y. Lee, Z. Salman, T. Prokscha, J.-M. Triscone, H. Y. Hwang, and A. Suter, Intrinsic magnetism in superconducting infinite-layer nickelates, *Nat. Phys.* **18**, 1043 (2022).
- [23] M. Rossi, M. O., J. Choi, S. Agrestini, D. Jost, Y. Lee, H. Lu, B. Y. Wang, K. Lee, A. Nag, Y.-D. Chuang, C.-T. Kuo, S.-J. Lee, B. Moritz, T. P. Devereaux, Z.-X. Shen, J.-S. Lee, K.-J. Zhou, H. Y. Hwang, and W.-S. Lee, A broken translational symmetry state in an infinite-layer nickelate, *Nat. Phys.* **18**, 869 (2022).
- [24] H. Sun, M. Huo, X. Hu, J. Li, Y. Han, L. Tang, Z. Mao, P. Yang, B. Wang, J. Cheng, D.-X. Yao, G.-M. Zhang, and M. Wang, Signatures of superconductivity near 80 K in a nickelate under high pressure, *Nature (London)* **621**, 493 (2023).
- [25] Y. Zhu, E. Zhang, B. Pan, X. Chen, D. Peng, L. Chen, H. Ren, F. Liu, N. Li, Z. Xing, J. Han, J. Wang, D. Jia, H. Wo, Y. Gu, Y. Gu, L. Ji, W. Wang, H. Gou, Y. Shen, T. Ying, X. Chen, W. Yang, C. Zheng, Q. Zeng, J.-G. Guo, and J. Zhao, Superconductivity in pressurized trilayer $\text{La}_4\text{Ni}_3\text{O}_{10-\delta}$ single crystals, *Nature (London)* **631**, 531 (2024).
- [26] Q. Li, Y.-J. Zhang, Z.-N. Xiang, Y. Zhang, X. Zhu, and H.-H. Wen, Signature of superconductivity in pressurized $\text{La}_4\text{Ni}_3\text{O}_{10}$, *Chin. Phys. Lett.* **41**, 017401 (2024).
- [27] Z. Liu, M. Huo, J. Li, Q. Li, Y. Liu, Y. Dai, X. Zhou, J. Hao, Y. Lu, M. Wang, and W.-H. Wen, Electronic correlations and partial gap in the bilayer nickelate $\text{La}_3\text{Ni}_2\text{O}_7$, *Nat. Commun.* **15**, 7570 (2024).
- [28] Y. Zhang, D. Su, Y. Huang, H. Sun, M. Huo, Z. Shan, K. Ye, Z. Yang, R. Li, M. Smidman, M. Wang, L. Jiao, and H. Yuan, High-temperature superconductivity with zero resistance and strange-metal behaviour in $\text{La}_3\text{Ni}_2\text{O}_{7-\delta}$, *Nat. Phys.* **20**, 1269 (2024).
- [29] J. Hou, P. T. Yang, Z. Y. Liu, J. Y. Li, P. F. Shan, L. Ma, G. Wang, N. N. Wang, H. Z. Guo, J. P. Sun, Y. Uwatoko, M. Wang, G.-M. Zhang, B. S. Wang, and J.-G. Cheng, Emergence of high-temperature superconducting phase in pressurized $\text{La}_3\text{Ni}_2\text{O}_7$ crystals, *Chin. Phys. Lett.* **40**, 117302 (2023).
- [30] J. Yang, H. Sun, X. Hu, Y. Xie, T. Miao, H. Luo, H. Chen, B. Liang, W. Zhu, G. Qu, C.-Q. Chen, M. Huo, Y. Huang, S. Zhang, F. Zhang, F. Yang, Z. Wang, Q. Peng, H. Mao, G. Liu, Z. Xu, T. Qian, D.-X. Yao, M. Wang, L. Zhao, and X. J. Zhou, Orbital-dependent electron correlation in double-layer nickelate $\text{La}_3\text{Ni}_2\text{O}_7$, *Nat. Commun.* **15**, 4373 (2024).
- [31] G. Wang, N. N. Wang, X. L. Shen, J. Hou, L. Ma, L. F. Shi, Z. A. Ren, Y. D. Gu, H. M. Ma, P. T. Yang, Z. Y. Liu, H. Z. Guo, J. P. Sun, G. M. Zhang, S. Calder, J.-Q. Yan, B. S. Wang, Y. Uwatoko, and J.-G. Cheng, Pressure-induced superconductivity in polycrystalline $\text{La}_3\text{Ni}_2\text{O}_{7-\delta}$, *Phys. Rev. X* **14**, 011040 (2024).
- [32] Z. Dong, M. Huo, J. Li, J. Li, P. Li, H. Sun, Y. Lu, M. Wang, Y. Wang, and Z. Chen, Visualization of oxygen vacancies and self-doped ligand holes in $\text{La}_3\text{Ni}_2\text{O}_{7-\delta}$, *Nature (London)* **630**, 847 (2024).
- [33] H. Sakakibara, M. Ochi, H. Nagata, Y. Ueki, H. Sakurai, R. Matsumoto, K. Terashima, K. Hirose, H. Ohta, M. Kato, Y. Takano, and K. Kuroki, Theoretical analysis on the possibility of superconductivity in the trilayer Ruddlesden-Popper nickelate $\text{La}_4\text{Ni}_3\text{O}_{10}$ under pressure and its experimental examination: Comparison with $\text{La}_3\text{Ni}_2\text{O}_7$, *Phys. Rev. B* **109**, 144511 (2024).
- [34] Y. Zhang, L.-F. Lin, A. Moreo, T. A. Maier, and E. Dagotto, Electronic structure, magnetic correlations, and superconducting pairing in the reduced Ruddlesden-Popper bilayer $\text{La}_3\text{Ni}_2\text{O}_6$ under pressure: Different role of $d_{3z^2-r^2}$ orbital compared with $\text{La}_3\text{Ni}_2\text{O}_7$, *Phys. Rev. B* **109**, 045151 (2024).
- [35] Y. Zhang, L.-F. Lin, A. Moreo, T. A. Maier, and E. Dagotto, Magnetic correlations and pairing tendencies of the hybrid stacking nickelate superlattice $\text{La}_7\text{Ni}_5\text{O}_{17}$ ($\text{La}_3\text{Ni}_2\text{O}_7/\text{La}_3\text{Ni}_4\text{O}_{10}$) under pressure, *Phys. Rev. B* **112**, 024508 (2025).

- [36] Y. Zhang, L.-F. Lin, A. Moreo, S. Okamoto, T. A. Maier, and E. Dagotto, Electronic structure, magnetic and pairing tendencies of alternating single-layer bilayer stacking nickelate $\text{La}_5\text{Ni}_3\text{O}_{11}$ under pressure, *Phys. Rev. B* (2025).
- [37] J.-X. Zhang, H.-K. Zhang, Y.-Z. You, and Z.-Y. Weng, Strong pairing originated from an emergent Z_2 Berry phase in $\text{La}_3\text{Ni}_2\text{O}_7$, *Phys. Rev. Lett.* **133**, 126501 (2024).
- [38] T. Xie, M. Huo, X. Ni, F. Shen, X. Huang, H. Sun, H. C. Walker, D. Adroja, D. Yu, B. Shen, L. He, K. Cao, and M. Wang, Strong interlayer magnetic exchange coupling in $\text{La}_3\text{Ni}_2\text{O}_{7-\delta}$ revealed by inelastic neutron scattering, *Sci. Bull.* **69**, 3221 (2024).
- [39] X. Chen, J. Choi, Z. Jiang, J. Mei, K. Jiang, J. Li, S. Agrestini, M. Garcia-Fernandez, X. Huang, H. Sun, D. Shen, M. Wang, J. Hu, Y. Lu, K.-J. Zhou, and D. Feng, Electronic and magnetic excitations in $\text{La}_3\text{Ni}_2\text{O}_7$, *Nat. Commun.* **15**, 9597 (2024).
- [40] Z. Dan, Y. Zhou, M. Huo, Y. Wang, L. Nie, M. Wang, T. Wu, and X. Chen, Pressure-enhanced spin-density-wave transition in double-layer nickelate $\text{La}_3\text{Ni}_2\text{O}_{7-\delta}$, *Sci. Bull.* **70**, 1239 (2025).
- [41] D. Takegami, K. Fujinuma, R. Nakamura, M. Yoshimura, K.-D. Tsuei, G. Wang, N. N. Wang, J.-G. Cheng, Y. Uwatoko, and T. Mizokawa, Absence of $\text{Ni}^{2+}/\text{Ni}^{3+}$ charge disproportionation and possible roles of O $2p$ holes in $\text{La}_3\text{Ni}_2\text{O}_{7-\delta}$ revealed by hard x-ray photoemission spectroscopy, *Phys. Rev. B* **109**, 125119 (2024).
- [42] S. Xu, C.-Q. Chen, M. Huo, D. Hu, H. Wang, Q. Wu, R. Li, D. Wu, M. Wang, D.-X. Yao, T. Dong, and N. Wang, Origin of the density wave instability in trilayer nickelate $\text{La}_4\text{Ni}_3\text{O}_{10}$ revealed by optical and ultrafast spectroscopy, *Phys. Rev. B* **111**, 075140 (2025).
- [43] K. Chen, X. Liu, J. Jiao, M. Zou, C. Jiang, X. Li, Y. Luo, Q. Wu, N. Zhang, Y. Guo, and L. Shu, Evidence of spin density waves in $\text{La}_3\text{Ni}_2\text{O}_{7-\delta}$, *Phys. Rev. Lett.* **132**, 256503 (2024).
- [44] N. Wang, G. Wang, X. Shen, J. Hou, J. Luo, X. Ma, H. Yang, L. Shi, J. Dou, J. Feng, J. Yang, Y. Shi, Z. Ren, H. Ma, P. Yang, Z. Liu, Y. Liu, H. Zhang, X. Dong, Y. Wang, K. Jiang, J. Hu, S. Nagasaki, K. Kitagawa, S. Calder, J. Yan, J. Sun, B. Wang, R. Zhou, Y. Uwatoko, and J. Cheng, Bulk high-temperature superconductivity in pressurized tetragonal $\text{La}_2\text{PrNi}_2\text{O}_7$, *Nature (London)* **634**, 579 (2024).
- [45] P. Lacorre, Passage from T-type to T'-type arrangement by reducing $\text{R}_4\text{Ni}_3\text{O}_{10}$ to $\text{R}_4\text{Ni}_3\text{O}_8$ ($R = \text{La}, \text{Pr}, \text{Nd}$), *J. Solid State Chem.* **97**, 495 (1992).
- [46] H. LaBollita and A. S. Botana, Electronic structure and magnetic properties of higher-order layered nickelates: $\text{La}_{n+1}\text{Ni}_n\text{O}_{2n+2}$ ($n = 4 - 6$), *Phys. Rev. B* **104**, 035148 (2021).
- [47] M.-C. Jung, J. Kapeghian, C. Hanson, B. Pamuk, and A. S. Botana, Electronic structure of higher-order Ruddlesden-Popper nickelates, *Phys. Rev. B* **105**, 085150 (2022).
- [48] C. D. Ling, D. N. Argyriou, G. Wu, and J. J. Neumeier, Neutron diffraction study of $\text{La}_3\text{Ni}_2\text{O}_7$: Structural relationships among $n = 1, 2$, and 3 phases $\text{La}_{n+1}\text{Ni}_n\text{O}_{3n+1}$, *J. Solid State Chem.* **152**, 517 (2000).
- [49] J. Li, P. Ma, H. Zhang, X. Huang, C. Huang, M. Huo, D. Hu, Z. Dong, C. He, J. Liao, X. Chen, T. Xie, H. Sun, M. Wang, Pressure-driven right-triangle shape superconductivity in bilayer nickelate $\text{La}_3\text{Ni}_2\text{O}_7$, *Nat. Sci. Rev.*, nwaf220 (2025).
- [50] M. Zhang, C. Pei, Q. Wang, Y. Zhao, C. Li, W. Cao, S. Zhu, J. Wu, and Y. Qi, Effects of pressure and doping on Ruddlesden-Popper phases $\text{La}_{n+1}\text{Ni}_n\text{O}_{3n+1}$, *J. Mater. Sci. Technol.* **185**, 147 (2024).
- [51] B. Geisler, J. J. Hamlin, G. R. Stewart, R. G. Hennig, and P. J. Hirschfeld, Structural transitions, octahedral rotations, and electronic properties of $\text{A}_3\text{Ni}_2\text{O}_7$ rare-earth nickelates under high pressure, *npj Quantum Mater.* **9**, 38 (2024).
- [52] L. Wang, L. Wang, Y. Li, S.-Y. Xie, F. Liu, H. Sun, C. Huang, Y. Gao, T. Nakagawa, B. Fu, B. Dong, Z. Cao, R. Yu, S. I. Kawaguchi, H. Kadobayashi, M. Wang, C. Jin, H.-K. Mao, and H. Liu, Structure responsible for the superconducting state in $\text{La}_3\text{Ni}_2\text{O}_7$ at high-pressure and low-temperature conditions, *J. Am. Chem. Soc.* **146**, 7506 (2024).
- [53] Y. Zhang, L.-F. Lin, A. Moreo, T. A. Maier, and E. Dagotto, Electronic structure, self-doping, and superconducting instability in the alternating single-layer trilayer stacking nickelates $\text{La}_3\text{Ni}_2\text{O}_7$, *Phys. Rev. B* **110**, L060510 (2024).
- [54] H. Sakakibara, N. Kitamine, M. Ochi, and K. Kuroki, Possible high T_c superconductivity in $\text{La}_3\text{Ni}_2\text{O}_7$ under high pressure through manifestation of a nearly half-filled bilayer Hubbard model, *Phys. Rev. Lett.* **132**, 106002 (2024).
- [55] J. Zhang, D. Phelan, A. S. Botana, Y.-S. Chen, H. Zheng, M. Krogstad, S. G. Wang, Y. Qiu, J. A. Rodriguez-Rivera, R. Osborn, S. Rosenkranz, M. R. Norman, and J. F. Mitchell, Intertwined density waves in a metallic nickelate, *Nat. Commun.* **11**, 6003 (2020).
- [56] H. Li, X. Zhou, T. Nummy, J. Zhang, V. Pardo, W. E. Pickett, J. F. Mitchell, and D. S. Dessau, Fermiology and electron dynamics of trilayer nickelate $\text{La}_4\text{Ni}_3\text{O}_{10}$, *Nat. Commun.* **8**, 704 (2017).
- [57] D. Puggioni and J. M. Rondinelli, Crystal structure stability and electronic properties of the layered nickelate $\text{La}_4\text{Ni}_3\text{O}_{10}$, *Phys. Rev. B* **97**, 115116 (2018).
- [58] J. Zhang, H. Zheng, Y.-S. Chen, Y. Ren, M. Yonemura, A. Huq, and J. F. Mitchell, High oxygen pressure floating zone growth and crystal structure of the metallic nickelates $\text{R}_4\text{Ni}_3\text{O}_{10}$ ($R = \text{La}, \text{Pr}$), *Phys. Rev. Mater.* **4**, 083402 (2020).
- [59] D. Rout, S. R. Mudi, M. Hoffmann, S. Spachmann, R. Klingeler, and S. Singh, Structural and physical properties of trilayer nickelates $\text{R}_4\text{Ni}_3\text{O}_{10}$ ($R = \text{La}, \text{Pr}$ and Nd), *Phys. Rev. B* **102**, 195144 (2020).
- [60] I. V. Leonov, Electronic structure and magnetic correlations in the trilayer nickelate superconductor $\text{La}_4\text{Ni}_3\text{O}_{10}$ under pressure, *Phys. Rev. B* **109**, 235123 (2024).
- [61] M. Zhang, C. Pei, D. Peng, X. Du, Y. Cao, Q. Wang, J. Wu, Y. Li, H. Liu, C. Wen, J. Song, Y. Zhao, C. Li, W. Cao, S. Zhu, Q. Zhang, N. Yu, P. Cheng, J. Zhao, Y. Chen, C. Jin, H. Guo, C. Wu, F. Yang, Q. Zeng, S. Yan, L. Yang, and Y. Qi, Superconductivity in trilayer nickelate $\text{La}_4\text{Ni}_3\text{O}_{10}$ under pressure, *Phys. Rev. X* **15**, 021005 (2025).
- [62] Y. Zhang, L.-F. Lin, A. Moreo, T. A. Maier, and E. Dagotto, Structural phase transition, s_{\pm} -wave pairing, and magnetic stripe order in bilayered superconductor $\text{La}_3\text{Ni}_2\text{O}_7$ under pressure, *Nat. Commun.* **15**, 2470 (2024).
- [63] V. Christiansson, F. Petocchi, and P. Werner, Correlated electronic structure of $\text{La}_3\text{Ni}_2\text{O}_7$ under pressure, *Phys. Rev. Lett.* **131**, 206501 (2023).
- [64] Q.-G. Yang, D. Wang, and Q.-H. Wang, Possible s^{\pm} -wave superconductivity in $\text{La}_3\text{Ni}_2\text{O}_7$, *Phys. Rev. B* **108**, L140505 (2023).

- [65] Y. Shen, M. Qin, and G.-M. Zhang, Effective bi-layer model Hamiltonian and density-matrix renormalization group study for the high- T_c superconductivity in $\text{La}_3\text{Ni}_2\text{O}_7$ under high pressure, *Chin. Phys. Lett.* **40**, 127401 (2023).
- [66] Y.-B. Liu, J.-W. Mei, F. Ye, W.-Q. Chen, and F. Yang, s^\pm -Wave pairing and the constructive role of apical-oxygen deficiencies in $\text{La}_3\text{Ni}_2\text{O}_7$ under pressure, *Phys. Rev. Lett.* **131**, 236002 (2023).
- [67] Y.-F. Yang, G.-M. Zhang, and F.-C. Zhang, Interlayer valence bonds and two-component theory for high- T_c superconductivity of $\text{La}_3\text{Ni}_2\text{O}_7$ under pressure, *Phys. Rev. B* **108**, L201108 (2023).
- [68] H. Oh and Y. H. Zhang, Type-II $t - J$ model and shared superexchange coupling from Hund's rule in superconducting $\text{La}_3\text{Ni}_2\text{O}_7$, *Phys. Rev. B* **108**, 174511 (2023).
- [69] Z. Liao, L. Chen, G. Duan, Y. Wang, C. Liu, R. Yu, and Q. Si, Electron correlations and superconductivity in $\text{La}_3\text{Ni}_2\text{O}_7$ under pressure tuning, *Phys. Rev. B* **108**, 214522 (2023).
- [70] Y. Cao and Y.-F. Yang, Flat bands promoted by Hund's rule coupling in the candidate double-layer high-temperature superconductor $\text{La}_3\text{Ni}_2\text{O}_7$, *Phys. Rev. B* **109**, L081105 (2024).
- [71] F. Lechermann, J. Gondolf, S. Bötzel, and I. M. Eremin, Electronic correlations and superconducting instability in $\text{La}_3\text{Ni}_2\text{O}_7$ under high pressure, *Phys. Rev. B* **108**, L201121 (2023).
- [72] D. A. Shilenko and I. V. Leonov, Correlated electronic structure, orbital-selective behavior, and magnetic correlations in double-layer under pressure, *Phys. Rev. B* **108**, 125105 (2023).
- [73] K. Jiang, Z. Wang, and F. Zhang, High-temperature superconductivity in $\text{La}_3\text{Ni}_2\text{O}_7$, *Chin. Phys. Lett.* **41**, 017402 (2024).
- [74] J. Huang, Z. D. Wang, and T. Zhou, Impurity and vortex states in the bilayer high-temperature superconductor $\text{La}_3\text{Ni}_2\text{O}_7$, *Phys. Rev. B* **108**, 174501 (2023).
- [75] Y. Zhang, L.-F. Lin, A. Moreo, T. A. Maier, and E. Dagotto, Trends in electronic structures and s^\pm -wave pairing for the rare-earth series in bilayer nickelate superconductors $R_3\text{Ni}_2\text{O}_7$, *Phys. Rev. B* **108**, 165141 (2023).
- [76] Q. Qin and Y.-F. Yang, High- T_c superconductivity by mobilizing local spin singlets and possible route to higher T_c in pressurized $\text{La}_3\text{Ni}_2\text{O}_7$, *Phys. Rev. B* **108**, L140504 (2023).
- [77] J.-X. Wang, Z. Ouyang, R.-Q. He, and Z.-Y. Lu, Non-Fermi liquid and Hund correlation in $\text{La}_4\text{Ni}_3\text{O}_{10}$ under high pressure, *Phys. Rev. B* **109**, 165140 (2024).
- [78] J. Li, C. Chen, C. Huang, Y. Han, M. Huo, X. Huang, P. Ma, Z. Qiu, J. Chen, X. Hu, L. Chen, T. Xie, B. Shen, H. Sun, D. Yao, and M. Wang, Structural transition, electric transport, and electronic structures in the compressed trilayer nickelate $\text{La}_4\text{Ni}_3\text{O}_{10}$, *Sci. Chin. Phys. Mech. Astron.* **67**, 117403 (2024).
- [79] Q.-G. Yang, K.-Y. Jiang, D. Wang, H.-Y. Lu, and Q.-H. Wang, Effective model and s^\pm -wave superconductivity in trilayer nickelate $\text{La}_4\text{Ni}_3\text{O}_{10}$, *Phys. Rev. B* **109**, L220506 (2024).
- [80] M. Zhang, H. Sun, Y.-B. Liu, Q. Liu, W.-Q. Chen, and F. Yang, s^\pm -wave superconductivity in pressurized $\text{La}_4\text{Ni}_3\text{O}_{10}$, *Phys. Rev. B* **110**, L180501 (2024).
- [81] J. Huang and T. Zhou, Interlayer pairing-induced partially gapped Fermi surface in trilayer $\text{La}_4\text{Ni}_3\text{O}_{10}$ superconductors, *Phys. Rev. B* **110**, L060506 (2024).
- [82] L.-F. Lin, Y. Zhang, N. Kaushal, G. Alvarez, T. A. Maier, A. Moreo, and E. Dagotto, Magnetic phase diagram of a two-orbital model for bilayer nickelates with varying doping, *Phys. Rev. B* **110**, 195135 (2024).
- [83] H. Oh, B. Zhou, and Y.-H. Zhang, Type-II $t - J$ model in charge transfer regime in bilayer $\text{La}_3\text{Ni}_2\text{O}_7$ and trilayer $\text{La}_4\text{Ni}_3\text{O}_{10}$, *Phys. Rev. B* **111**, L020504 (2025).
- [84] M. Zhang, H. Sun, Y.-B. Liu, Q. Liu, W.-Q. Chen, and F. Yang, Spin-density wave and superconductivity in $\text{La}_4\text{Ni}_3\text{O}_{10}$ under ambient pressure, *Phys. Rev. B* **111**, 144502 (2025).
- [85] J. Chen, F. Yang, and W. Li, Orbital-selective superconductivity in the pressurized bilayer nickelate $\text{La}_3\text{Ni}_2\text{O}_7$: An infinite projected entangled-pair state study, *Phys. Rev. B* **110**, L041111 (2024).
- [86] S. Ryege, N. Witt, and T. O. Wehling, Quenched pair breaking by interlayer correlations as a key to superconductivity in $\text{La}_3\text{Ni}_2\text{O}_7$, *Phys. Rev. Lett.* **133**, 096002 (2024).
- [87] G. Heier, K. Park, and S. Y. Savrasov, Competing d_{xy} and s^\pm pairing symmetries in superconducting $\text{La}_3\text{Ni}_2\text{O}_7$: LDA+FLEX calculations, *Phys. Rev. B* **109**, 104508 (2024).
- [88] J. Zhan, Y. Gu, X. Wu, and J. Hu, Cooperation between electron-phonon coupling and electronic interaction in bilayer nickelates $\text{La}_3\text{Ni}_2\text{O}_7$, *Phys. Rev. Lett.* **134**, 136002 (2025).
- [89] B. Geisler, L. Fanfarillo, J. J. Hamlin, G. R. Stewart, R. G. Hennig, and P. J. Hirschfeld, Optical properties and electronic correlations in $\text{La}_3\text{Ni}_2\text{O}_7$ bilayer nickelates under high pressure, *npj Quantum Mater.* **9**, 89 (2024).
- [90] H. LaBollita, V. Pardo, M. R. Norman, and A. S. Botana, Assessing spin-density wave formation in $\text{La}_3\text{Ni}_2\text{O}_7$ from electronic structure calculations, *Phys. Rev. Mater.* **8**, L111801 (2024).
- [91] M. Lu and T. Zhou, Assessing spin-density wave formation in $\text{La}_3\text{Ni}_2\text{O}_7$ from electronic structure calculations, *Phys. Rev. B* **111**, 094504 (2025).
- [92] G. Duan, Z. Liao, L. Chen, Y. Wang, R. Yu, and Q. Si, Orbital-selective correlation effects and superconducting pairing symmetry in a multiorbital $t - J$ model for bilayer nickelates, *arXiv:2502.09195*.
- [93] L. B. Braz, G. B. Martins, and L. G. G. V. Dias da Silva, Interlayer interactions in $\text{La}_3\text{Ni}_2\text{O}_7$ under pressure: From s^\pm to d_{xy} -wave superconductivity, *Phys. Rev. Res.* **7**, 033023 (2025).
- [94] Y.-F. Yang, Decomposition of multilayer superconductivity with interlayer pairing, *Phys. Rev. B* **110**, 104507 (2024).
- [95] Z. Luo, X. Hu, M. Wang, W. Wu, and D.-X. Yao, Bilayer two-orbital model of $\text{La}_3\text{Ni}_2\text{O}_7$ under pressure, *Phys. Rev. Lett.* **131**, 126001 (2023).
- [96] Y. Zhang, L.-F. Lin, A. Moreo, and E. Dagotto, Electronic structure, dimer physics, orbital-selective behavior, and magnetic tendencies in the bilayer nickelate superconductor $\text{La}_3\text{Ni}_2\text{O}_7$ under pressure, *Phys. Rev. B* **108**, L180510 (2023).
- [97] Y. Zhang, L.-F. Lin, A. Moreo, T. A. Maier, and E. Dagotto, Prediction of s^\pm -wave superconductivity enhanced by electronic doping in trilayer nickelates $\text{La}_4\text{Ni}_3\text{O}_{10}$ under pressure, *Phys. Rev. Lett.* **133**, 136001 (2024).
- [98] H. LaBollita, J. Kapeghian, M. R. Norman, and A. S. Botana, Electronic structure and magnetic tendencies of trilayer $\text{La}_4\text{Ni}_3\text{O}_{10}$ under pressure: Structural transition, molecular orbitals, and layer differentiation, *Phys. Rev. B* **109**, 195151 (2024).
- [99] X.-Z. Qu, D.-W. Qu, J. Chen, C. Wu, F. Yang, W. Li, and G. Su, Bilayer $t - J - J_\perp$ model and magnetically mediated pairing

- in the pressurized nickelate $\text{La}_3\text{Ni}_2\text{O}_7$, *Phys. Rev. Lett.* **132**, 036502 (2024).
- [100] C. Lu, Z. Pan, F. Yang, and C. Wu, Interlayer-coupling-driven high-temperature superconductivity in $\text{La}_3\text{Ni}_2\text{O}_7$ under pressure, *Phys. Rev. Lett.* **132**, 146002 (2024).
- [101] Y.-H. Tian, Y. Chen, J.-M. Wang, R.-Q. He, and Z.-Y. Lu, Correlation effects and concomitant two-orbital s_{\pm} -wave superconductivity in $\text{La}_3\text{Ni}_2\text{O}_7$ under high pressure, *Phys. Rev. B* **109**, 165154 (2024).
- [102] H. Liu, C. Xia, S. Zhou, H. Chen, Sensitive dependence of pairing symmetry on Ni-eg crystal field splitting in the nickelate superconductor $\text{La}_3\text{Ni}_2\text{O}_7$, *Nat. Commun.* **16**, 1054 (2025).
- [103] Z. Fan, J.-F. Zhang, B. Zhan, D. Lv, X.-Y. Jiang, B. Normand, and T. Xiang, Superconductivity in nickelate and cuprate superconductors with strong bilayer coupling, *Phys. Rev. B* **110**, 024514 (2024).
- [104] E. Dagotto, J. Riera, and D. Scalapino, Superconductivity in ladders and coupled planes, *Phys. Rev. B* **45**, 5744(R) (1992).
- [105] G. Kresse and J. Hafner, *Ab initio* molecular dynamics for liquid metals, *Phys. Rev. B* **47**, 558 (1993).
- [106] G. Kresse and J. Furthmüller, Generalized gradient approximation made simple, *Phys. Rev. B* **54**, 11169 (1996).
- [107] P. E. Blöchl, Projector augmented-wave method, *Phys. Rev. B* **50**, 17953 (1994).
- [108] J. P. Perdew, K. Burke, and M. Ernzerhof, Generalized gradient approximation made simple, *Phys. Rev. Lett.* **77**, 3865 (1996).
- [109] A. A. Mostofi, J. R. Yates, Y. S. Lee, I. Souza, D. Vanderbilt, and N. Marzari, wannier90: A tool for obtaining maximally-localised Wannier functions, *Comput. Phys. Commun.* **178**, 685 (2008).
- [110] K. Momma and F. Izumi, VESTA 3 for three-dimensional visualization of crystal, volumetric and morphology data, *J. Appl. Crystallogr.* **44**, 1272 (2011).
- [111] See Supplemental Material at <http://link.aps.org/supplemental/10.1103/h9kq-chh7> for detailed hopping matrices and crystal-field splitting.
- [112] S. Graser, T. A. Maier, P. J. Hirschfeld, and D. J. Scalapino, Near-degeneracy of several pairing channels in multiorbital models for the Fe pnictides, *New J. Phys.* **11**, 025016 (2009).
- [113] K. Kubo, Pairing symmetry in a two-orbital Hubbard model on a square lattice, *Phys. Rev. B* **75**, 224509 (2007).
- [114] A. T. Rømer, T. A. Maier, A. Kreisel, I. Eremin, P. J. Hirschfeld, and B. M. Andersen, Pairing in the two-dimensional Hubbard model from weak to strong coupling, *Phys. Rev. Res.* **2**, 013108 (2020).
- [115] M. Altmeyer, D. Guterding, P. J. Hirschfeld, T. A. Maier, R. Valentí, and D. J. Scalapino, Role of vertex corrections in the matrix formulation of the random phase approximation for the multiorbital Hubbard model, *Phys. Rev. B* **94**, 214515 (2016).
- [116] V. Mishra, T. A. Maier, and D. J. Scalapino, s^{\pm} pairing near a Lifshitz transition, *Sci. Rep.* **6**, 32078 (2016).
- [117] T. A. Maier and E. Dagotto, Coupled Hubbard ladders at weak coupling: Pairing and spin excitations, *Phys. Rev. B* **105**, 054512 (2022).
- [118] S. V. Streltsov and D. I. Khomskii, Orbital-dependent singlet dimers and orbital-selective Peierls transitions in transition-metal compounds, *Phys. Rev. B* **89**, 161112(R) (2014).
- [119] Y. Zhang, L. F. Lin, A. Moreo, and E. Dagotto, Orbital-selective Peierls phase in the metallic dimerized chain MoOCl_2 , *Phys. Rev. B* **104**, L060102 (2021).
- [120] P. Li, G. Zhou, W. Lv, Y. Li, C. Yue, H. Huang, L. Xu, J. Shen, Y. Miao, W. Song, Z. Nie, Y. Chen, H. Wang, W. Chen, Y. Huang, Z.-H. Chen, T. Qian, J. Lin, J. He, Y.-J. Sun, Z. Chen, and Q.-K. Xue, Angle-resolved photoemission spectroscopy of superconducting $(\text{La}, \text{Pr})_3\text{Ni}_2\text{O}_7/\text{SrLaAlO}_4$ heterostructures, *Natl. Sci. Rev.* **1**, nwaf205 (2025).
- [121] C.-Q. Chen, Z. Luo, M. Wang, W. Wu, and D.-X. Yao, Trilayer multiorbital models of $\text{La}_4\text{Ni}_3\text{O}_{10}$, *Phys. Rev. B* **110**, 014503 (2024).
- [122] Z. Luo, B. Lv, M. Wang, W. Wu, and D.-X. Yao, High- T_C superconductivity in $\text{La}_3\text{Ni}_2\text{O}_7$ based on the bilayer two-orbital t-J model, *npj Quantum Mater.* **9**, 61 (2024).
- [123] S. Fan, M. Ou, M. Scholten, Q. Li, Z. Shang, Y. Wang, J. Xu, H. Yang, I. M. Eremin, and H.-H. Wen, Superconducting gaps revealed by STM measurements on $\text{La}_2\text{PrNi}_2\text{O}_7$ thin films at ambient pressure, [arXiv:2506.01788](https://arxiv.org/abs/2506.01788).
- [124] Q. Gu, Y. Li, S. Wan, H. Li, W. Guo, H. Yang, Q. Li, X. Zhu, X. Pan, Y. Nie, and H.-H. Weno, Single particle tunneling spectrum of superconducting $\text{Nd}_{1-x}\text{Sr}_x\text{NiO}_2$ thin films, *Nat. Commun.* **11**, 6027 (2020).
- [125] L. F. Lin, Y. Zhang, G. Alvarez, A. Moreo, and E. Dagotto, Origin of insulating ferromagnetism in iron oxychalcogenide $\text{Ce}_2\text{O}_2\text{FeSe}_2$, *Phys. Rev. Lett.* **127**, 077204 (2021).
- [126] L. F. Lin, Y. Zhang, G. Alvarez, M. A. McGuire, A. F. May, A. Moreo, and E. Dagotto, Stability of the interorbital-hopping mechanism for ferromagnetism in multi-orbital Hubbard models, *Commun. Phys.* **6**, 199 (2023).
- [127] L. F. Lin, Y. Zhang, G. Alvarez, A. Moreo, Jacek Herbrych, and E. Dagotto, Prediction of orbital-selective Mott phases and block magnetic states in the quasi-one-dimensional iron chain $\text{Ce}_2\text{O}_2\text{FeSe}_2$ under hole and electron doping, *Phys. Rev. B* **105**, 075119 (2022).
- [128] Q. Qin, J. Wang, Y.-F. Yang, Frustrated superconductivity and intrinsic reduction of T_c in trilayer nickelate, *Innovat. Mater.* **2**, 100102 (2024).
- [129] P. G. Freeman, M. Enderle, S. M. Hayden, C. D. Frost, D. X. Yao, E. W. Carlson, D. Prabhakaran, and A. T. Boothroyd, Inward dispersion of the spin excitation spectrum of stripe-ordered $\text{La}_2\text{NiO}_{4+\delta}$, *Phys. Rev. B* **80**, 144523 (2009).
- [130] D. X. Yao and E. W. Carlson, Spin-wave dispersion in half-doped $\text{La}_{3/2}\text{Sr}_{1/2}\text{NiO}_4$, *Phys. Rev. B* **75**, 012414 (2007).
- [131] G. Zhou, F. Jiang, J. Zang, Z. Quan, and X. Xu, Observation of superconductivity in the $\text{LaNiO}_3/\text{La}_{0.7}\text{Sr}_{0.3}\text{MnO}_3$ superlattice, *ACS Appl. Mater. Interfaces* **10**, 1463 (2018).
- [132] Y. Gao, W. Wu, Z. Liu, K. Held, and L. Si, Topotactical hydrogen induced single-band d -wave superconductivity in LaNiO_4 , *Phys. Rev. Lett.* **135**, 026002 (2025).
- [133] Z. Li, W. Guo, T. T. Zhang, J. H. Song, T. Y. Gao, Z. B. Gu, and Y. F. Nie, Epitaxial growth and electronic structure of Ruddlesden-Popper nickelates $(\text{La}_{3n+1}\text{Ni}_n\text{O}_{3n+1})$ ($n = 1 - 5$), *APL Mater.* **8**, 091112 (2020).
- [134] W. Sun, Y. Li, X. Cai, J. Yang, W. Guo, Z. Gu, Y. Zhu, and Y. Nie, Electronic and transport properties in Ruddlesden-Popper neodymium nickelates $\text{Nd}_{3n+1}\text{Ni}_n\text{O}_{3n+1}$ ($n = 1 - 5$), *Phys. Rev. B* **104**, 184518 (2021).
- [135] M. Osada, C. Terakura, A. Kikkawa, M. Nakajima, H.-Y. Chen, Y. Nomura, Y. Tokura, and A. Tsukazaki, Strain-tuning

- for superconductivity in $\text{La}_3\text{Ni}_2\text{O}_7$ thin films, *Commun. Phys.* **8**, 251 (2025).
- [136] M. Shi, D. Peng, K. Fan, Z. Xing, S. Yang, Y. Wang, H. Li, R. Wu, M. Du, B. Ge, Z. Zeng, Q. Zeng, J. Ying, T. Wu, and X. Chen, Pressure induced superconductivity in hybrid Ruddlesden–Popper $\text{La}_5\text{Ni}_3\text{O}_{11}$ single crystals, *Nat. Phys.* (2025), doi:[10.1038/s41567-025-03023-3](https://doi.org/10.1038/s41567-025-03023-3).
- [137] Y.-F. Zhao and A. S. Botana, Electronic structure of Ruddlesden-Popper nickelates: Strain to mimic the effects of pressure, *Phys. Rev. B* **111**, 115154 (2025).
- [138] <https://www.energy.gov/doi-public-access-plan>.
- [139] <https://doi.org/10.5281/zenodo.17048362>.
- [140] <https://github.com/maiertar/MPAPP>.
- [141] S. L. Dudarev, G. A. Botton, S. Y. Savrasov, C. J. Humphreys, and A. P. Sutton, Electron-energy-loss spectra and the structural stability of nickel oxide: An LSDA+U study, *Phys. Rev. B* **57**, 1505 (1998).